POLITECNICO
MILANO 1863

SCUOLA DI INGEGNERIA INDUSTRIALE
E DELL'INFORMAZIONE

Design Aspects of Direct Drive Permanent Magnet Machines For Wind Power Generation

TESI DI LAUREA MAGISTRALE IN
ELECTRICAL ENGINEERING
INGEGNERIA ELETTRICA

Author: **Abdul Samad**

Student ID: 10801316
Advisor: Professor Antonino Di Gerlando
Academic Year: 2022-23

Abstract

Clean energy is necessary for the long-term growth of the sustainable society. Wind energy is rapidly expanding and contributes to many countries' efforts to decrease greenhouse gas emissions. In the wind power industry, the debate on which generator and converter option makes for the best modern wind turbine drive trains is still going strongly. In this thesis we discussed the various aspects of PM machines for wind power Industry.

Different type of generators are discussed and design aspects of permanent magnet machines also have been highlighted like mechanical structure, thermal behaviour and electromagnetic structure. In the end we will see the brief discussion about the 2MW direct drive train for wind turbine and its characteristics. In mechanical point of view, the solution for reducing the mechanical structure, DDPM for large wind turbines is to do without a shaft and torque arms. In thermal aspects, some main parameters for design like polar arc coefficient and air gap length on various parts of AFPM and RFPM were compared and studied, and we can conclude that, variations in heat source and thermal resistance are the fundamental causes of temperature changes. The majority of the characteristics used as the study object in this work have an impact on both the heat source and thermal resistance. For Electromagnetic design, we discussed both static and dynamic operation of PM machines and also some of the machine performance aspects.

Key-words: Permanent Magnet Machines, Wind Power Generation, PMSG, Direct Drive Permanent Magnet

Abstract in italiano

L'energia pulita è necessaria per la crescita a lungo termine della società sostenibile. L'energia eolica è in rapida espansione e contribuisce agli sforzi di molti paesi per ridurre le emissioni di gas serra. Nel settore dell'energia eolica, il dibattito su quale opzione generatore e convertitore costituisca la migliore trasmissione per turbine eoliche moderne è ancora in corso. In questa tesi abbiamo discusso i vari aspetti delle macchine magneti permanenti per l'industria eolica.

Vengono discussi diversi tipi di generatori e sono stati evidenziati anche gli aspetti di progettazione delle macchine a magneti permanenti come la struttura meccanica, il comportamento termico e la struttura elettromagnetica. Alla fine, vedremo la breve discussione sulla trasmissione diretta da 2 MW per turbina eolica e le sue caratteristiche. Dal punto di vista meccanico, la soluzione per ridurre la struttura meccanica, Magnete permanente a trasmissione diretta per grandi turbine eoliche è fare a meno di albero e bracci di reazione. Per quanto riguarda gli aspetti termici, sono stati confrontati e studiati alcuni parametri principali per la progettazione come il coefficiente dell'arco polare e la lunghezza del traferro su varie parti di Magnete permanente a flusso assiale e Magnete permanente a flusso radiale, e possiamo concludere che le variazioni nella fonte di calore e nella resistenza termica sono le cause fondamentali dei cambiamenti di temperatura. La maggior parte delle caratteristiche utilizzate come oggetto di studio in questo lavoro hanno un impatto sia sulla fonte di calore che sulla resistenza termica. Per la progettazione elettromagnetica, abbiamo discusso sia il funzionamento statico che dinamico delle macchine magnete permanente e anche alcuni aspetti delle prestazioni della macchina.

Parole chiave: Macchine a magneti permanenti, Generazione di energia eolica, PMSG, Magnete permanente a trasmissione diretta

Acknowledgments

I would like to thank my Prof. Antonino Di Gerlando for his continuous support for my MSc study and research, for his patience and motivation towards the work.

I am grateful to Politecnico di Milano for my masters degree experience and the opportunities which the university has provided.

I am eternally thankful and grateful to my parents, my dear wife, and sisters for the encouragement throughout this unforgettable journey. A big thank you for your love and support.

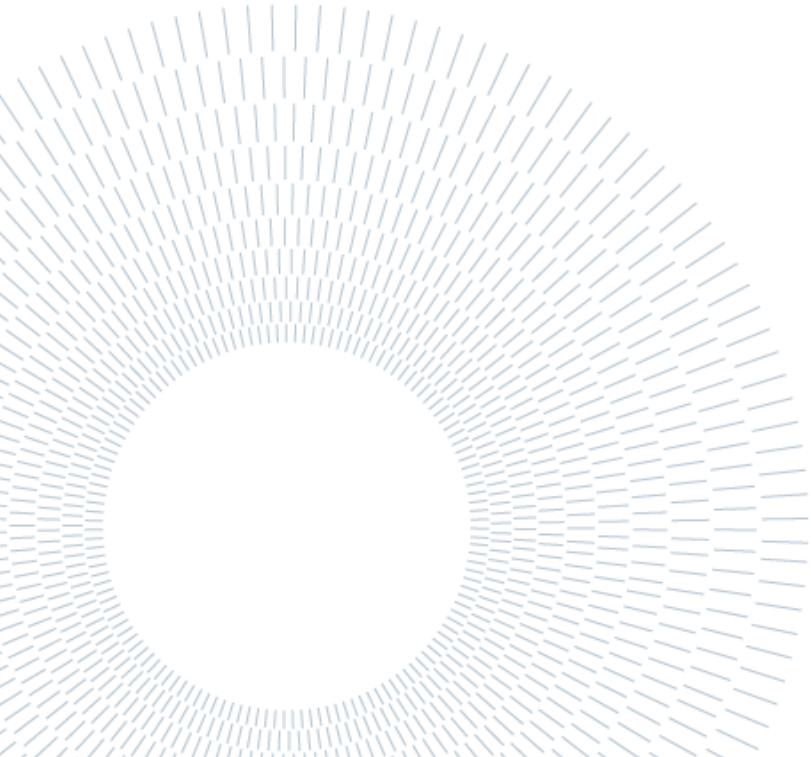

Table of Contents

List of Figures

List of Tables

List of Acronyms

PMSG – Permanent Magnet Synchronous Generator

EESG –Electrically Excited Synchronous Generator

DDPMSG – Direct Drive Permanent Magnet Synchronous Generator

DDPM – Direct Drive Permanent Magnet

PMG – Permanent Magnet Generator

AFPM – Axial Flux Permanent Magnet

RFPM – Radial Flux Permanent Magnet

TFM –Transverse Flux Machine

TFPM – Transverse Flux Permanent Magnet

PWM – Pulse Width Modulation

FE – Finite Element

EMF – Electromotive Force

MMF – Magnetivemotive Force

ENTM – Equivalent Thermal Network Model

1 Introduction To Wind Power Generation

1.1. Wind Power Generation

A wind turbine first converts the kinetic energy of the wind into mechanical rotational energy and then into electrical energy. A turbine can be divided into three main parts: the tower, the rotor, and the nacelle. The tower is the supporting structure of the wind turbine. The rotor, i.e. the blades and the hub, transfers the mechanical energy to the nacelle. Depending on the orientation of the rotor, two types of wind turbines can be distinguished: Upwind and downwind turbines. In the upwind turbine, the rotor faces the wind, while in the downwind turbine, the rotor is located downwind of the tower (see figure 1). The nacelle contains the electrical generator, gearbox (if present), controls, and brake. The components of the nacelle serve as converters; they convert the rotational energy of the rotor hub into electrical energy.

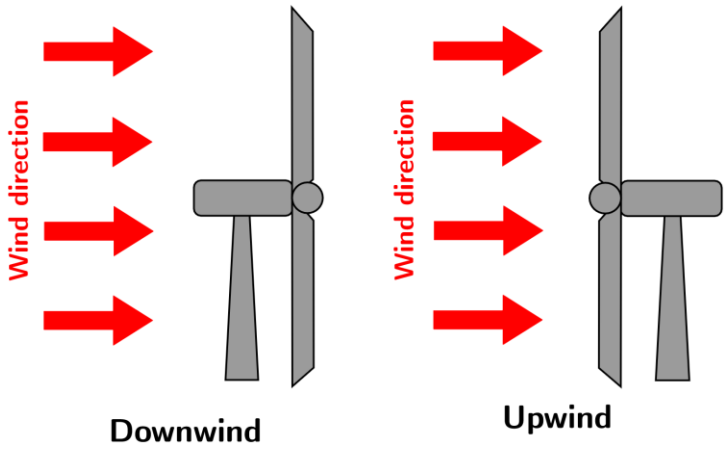

Figure 1 Upwind and Downwind Wind Turbines

The total power delivered by a wind turbine differs with respect to the wind speed and characteristic power performance curve of this turbine. The amount of the power extracted by the wind turbine is proportional to its swept area A (m2) ((A = *p* r2) r is the radius of the swept area, which represents also the blade's length), the air density *r*air (kg/m3) (i.e., mass per unit of volume) and to the cube of the wind velocity vair (m/s) reduced by power coefficient Cp according to the formula:

$$P_{Tubine} = \underbrace{\frac{1}{2}\rho_{air}(z)\, A_z\, v_{air}^3}_{P_{wind}}\, C_p(\beta, \lambda) \quad (1)$$

where Pwind (W) is the available power in wind, Cp is the power coefficient, which is a measure of aerodynamic efficiency of extracting energy from the wind, and z (m) denotes the altitude above the sea. λ and β are the tip–speed ratio and the pitch angle (will be further detailed). It should be noted that the air density varies as a function of temperature and pressure in compliance with the perfect gas law. Since both pressure and temperature depend on the altitude above the sea level, the air density can be expressed by:

$$\rho_{air}(z) = \frac{P_0}{RT} e^{\frac{-gz}{RT}} \quad (2)$$

where P0 is the standard sea level atmospheric density (1.225 kg/m3);

R is the specific gas constant for air (287.05 J/kg/K);

g is the gravity constant (9.81 m.s−2);

T is the temperature (K);

z is the altitude above sea level (m).

The power coefficient represents the aerodynamic efficiency of the wind turbine; it is a measurement of how efficiently the wind turbine extracts the wind energy (in the airflow). This coefficient depends on the aerodynamic air foil shape, chord length, blade length, and blade twist. Furthermore, the overall wind turbine efficiency depends on the aerodynamic, mechanical (gearbox, shaft bearing support) and electrical (generator, converter) inefficiencies. The theoretical maximum value of the power coefficient is defined by Betz's Law, which states that the maximum captured power by the wind turbine could not exceed 16/27 (59.3%) of the available wind power wind [1]. However, Cp is usually less than 45%. This significant reduction in the power coefficient is due to the presence of aerodynamic losses in the wind turbine systems such as the blade tips, blade roots, and wake losses. Fortunately, advances in technology allow modern wind turbines to operate near to the theoretical limit. Cp could be expressed as a function of the tip–speed ratio λ and the pitch angle β; the curve relating those coefficients could be best obtained from direct measurements of the turbine in operation [2]. The TSR refers to the ratio between the rotor tip speed (linear speed of the rotor tip) and the wind speed:

$$\lambda = \frac{\omega_r r}{v} = \frac{v_r}{v} \quad (3)$$

where ωr (rad/s) (ωr = 2π f) is rotor tip angular velocity , f (Hz) is the blade frequency, and υr is the rotational speed of the blades (speed of the blades ends). It is therefore essential to calculate the optimal tip speed to maximize the turbine's efficiency [3]. For a given wind turbine, the power coefficient depends on both the tip speed ratio and pitch angle. The characteristic curves in Figure 2 illustrate the interrelationship between Cp and λ for different values of pitch angle. For a particular value of λ, the power coefficient increases with the decrease of β, and thus, the maximum of the power coefficient is achieved for zero pitch angle (0 degree). For a given pitch angle, it could be seen that the Cp increases with the increase in the tip–speed ratio until it reaches its maximum at λopt, and then, it starts to decline steadily with a further increase in λ.

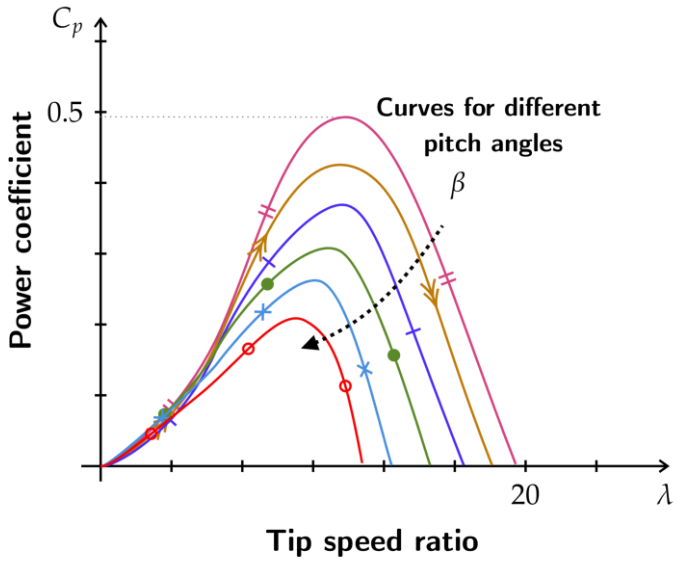

Figure 2 Power coefficient with respect to the pitch angle and tip speed ratio Cp(λ, β).

The efficiency of the wind turbine is not constant, and it depends on the wind speed. Thus, the power curve could be split into four operation regions with respect to the wind speed.

• Region I: when the wind speed is less than the threshold speed, the torque is insufficient to overcome the power loss (i.e., losses due to drag at the blade, friction losses in the gearbox and in bearings, electrical losses with the generator); therefore, no power is generated below the cut-in speed.

• Region II: (variable speed region) when the wind speed exceeds the cut-in speed (around 3–5 m/s depending on the turbine design), there is a sufficient torque for rotation; thus, the turbine starts to generate electricity. In this operational mode, which accounted for more than 50% of the yearly energy capture for a typical modern wind turbine [4], the power produced by the wind turbine increases proportionally to the cubic power of the wind speed (as is expected from (1)). The power curve reaches a

peak around the so-called rated output speed (12–14 m/s). Above the rated output speed, the power generated remains unchanged at its permanently permissible maximum (known as rated power); it is kept almost constant by different control options. The pitch angle is usually controlled to keep the wind turbine operating at the peak of the Cp–TSR–pitch surface [4] and to limit the power when the speed exceeded the rated wind speed to avoid structural failure [5].

• Region III: (constant speed region) at which the wind speed is between rated speed and cut out speed (around 25 m/s). The rotor speed is held constant above the rated speed by the regulation of the angle of attack (See Figure 2). This ensures limited aerodynamic power in this region despite much more available wind energy.

• Region VI: When the wind speed exceeds the cut-out speed, the wind turbine is shut down.

1.2. Wind Turbine Types

Wind Turbines have the basic components as shown in Fig 3. and Wind Turbine comes with various types and topologies and can be categorized with different things like,

• Rotor axis orientation: horizontal or vertical

• Rotor position: upwind or downwind of tower

• Rotor speed: fixed or variable

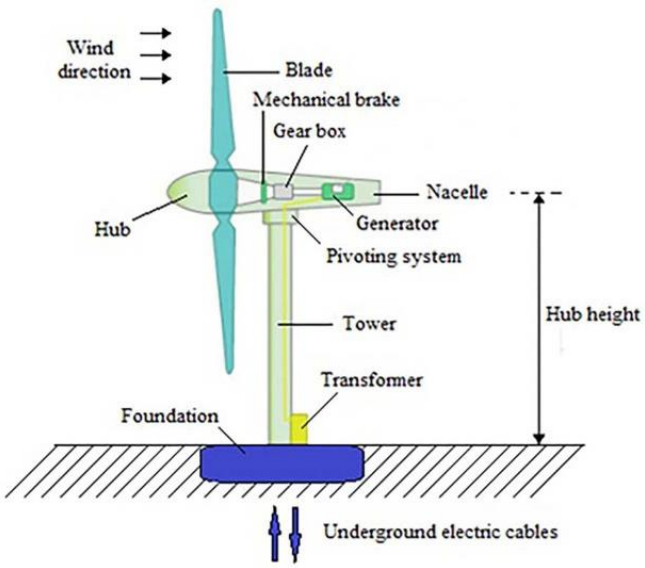

Figure 3 Components of Wind Turbine Power Generation

Here some of the categories are discussed below

1.2.1. Rotor Axis Orientation

- Horizontal Axis Wind Turbine (HAWT)
- Vertical Axis Wind Turbines (VAWT)

Horizontal Axis Wind Turbine (HAWT)

Horizontal axis wind turbines are the most commonly used turbines due to their strength and efficiency. The base of the towers have to be extremely strong, allowing the rotor shaft to be installed at the top of the tower which allows the turbine to be exposed to stronger winds. With the blades of the turbine being perpendicular to the wind, the rotation of the blades can generate more power compared to the vertical axis wind turbine. However, the construction of this type of turbine requires a heavy support for the tower to support the weight of the blades, gearbox and generator as well as utilizing a sizable crane to lift the components to the top of the tower. [8]

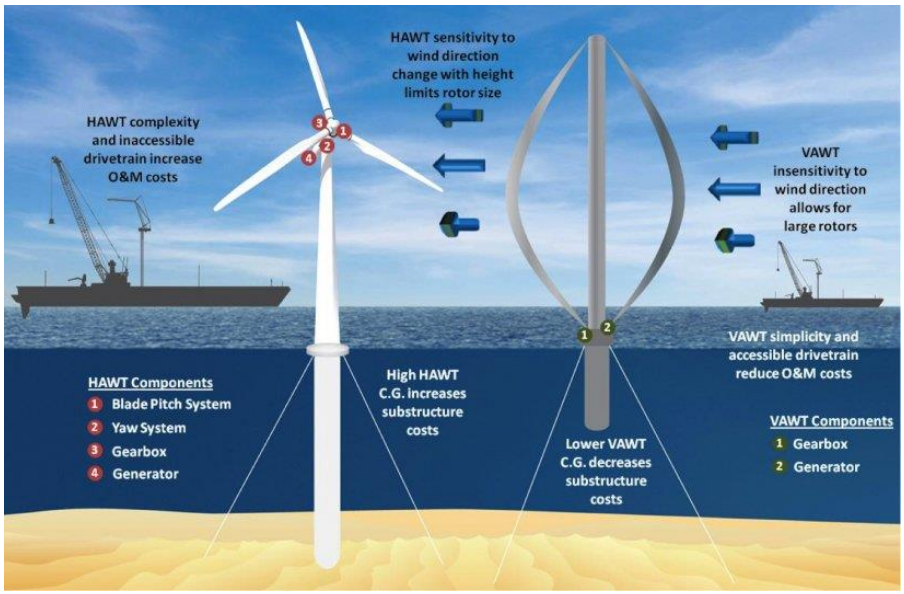

Figure 4 Types of Turbines

Vertical Axis Wind Turbine (VAWT)

Vertical axis wind turbines are less affected by frequent wind direction changes as compared to the horizontal axis wind turbines due to the blades being rotated on the rotor shaft perpendicular to the ground. With the blades and shaft installed in this way, the turbine does not need to rotate to track wind direction. The shaft is mounted near ground level due to the difficulties of mounting the shaft and its components on the tower. An advantage of being mounted at ground level is that maintenance of the

turbine is easier and can be installed at locations such as rooftops. Disadvantages to this turbine installation is that the efficiency is lower due to air drag and the lower wind speeds compared to the higher wind speeds encountered at higher elevation [8]

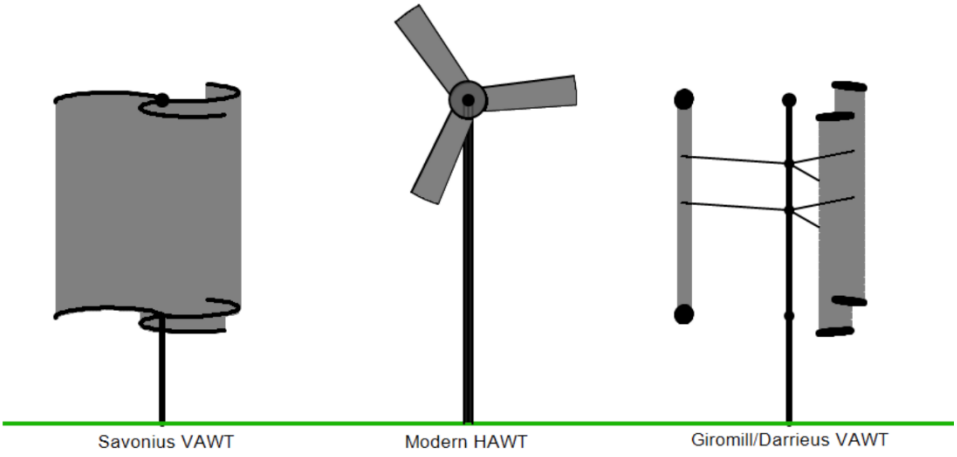

Figure 5 Types of Vertical Axis Turbines

1.2.2. Rotor Position

Upwind Turbines

Upwind machines have the rotor facing the wind. The basic advantage of upwind designs is that one avoids the wind shade behind the tower. By far the vast majority of wind turbines have this design.

On the other hand, there is also some wind shade in front of the tower, i.e. the wind starts bending away from the tower before it reaches the tower itself, even if the tower is round and smooth. Therefore, each time the rotor passes the tower, the power from the wind turbine drops slightly.

The basic drawback of upwind designs is that the rotor needs to be made rather inflexible and placed at some distance from the tower (as some manufacturers have found out to their cost). In addition, an upwind machine needs a yaw mechanism to keep the rotor facing the wind. [9]

Downwind Turbines

Downwind machines have the rotor placed on the lee side of the tower. They have the theoretical advantage that they may be built without a yaw mechanism, if the rotor and nacelle have a suitable design that makes the nacelle follow the wind passively. For large wind turbines this is a somewhat doubtful advantage, however, since you do need cables to lead the current away from the generator. How do you untwist the cables, when the machine has been yawing passively in the same direction for a long period of time, if you do not have a yaw mechanism? (Slip rings or mechanical collectors are not a very good idea if you are working with 1000 ampere currents).

A more important advantage is that the rotor may be made more flexible. This is an advantage both in regard to weight, and the structural dynamics of the machine, i.e. the blades will bend at high wind speeds, thus taking part of the load off the tower. The basic advantage of the downwind machine is thus, that it may be built somewhat lighter than an upwind machine.

The basic drawback is the fluctuation in the wind power due to the rotor passing through the wind shade of the tower. This may give more fatigue loads on the turbine than with an upwind design. [9]

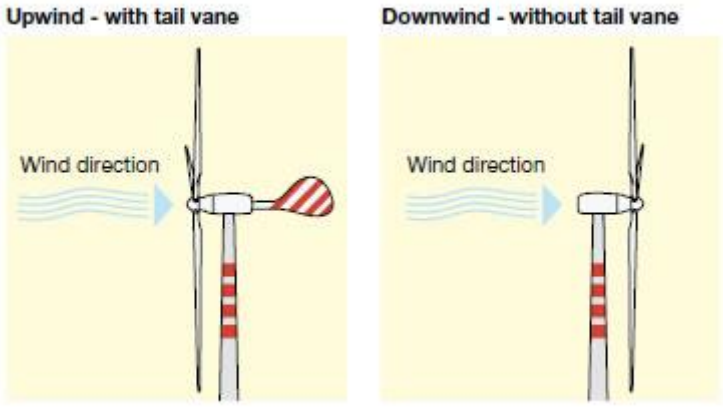

Figure 6 Types of Wind Turbine According to Rotor Position

1.2.3. Rotor Speed

Variable Speed Wind Turbine

For variable speed machine the mechanical conversion efficiency can be made high limited only in higher wind speed limit. In high-speed limit (>=11.54 m/sec) with the help of control of turbine combined with controller action, generator speed is not allowed to increase beyond 1.02 p.u. corresponding to 50 Hz. stator frequency.

Fixed Speed Wind Turbine

For fixed speed machine the frequency or speed dependant loss (Hysteresis, Frictional loss of Gear, and Frictional and windage loss of Generator) is almost constant But in Variable Speed Machine, above losses reduce with fall of frequency/speed hence net losses are lower.

1.3. Generation System in Wind Turbines

Generator is one of the most important components of a wind energy conversion system (second important component), generator of a wind turbine has to work under fluctuating power levels. Different types of generators are being used with wind turbines. These generators can either be induction (asynchronous) generators or synchronous generators and recently appeared innovative machine

1.3.1. Squirrel-Cage Induction Generator (SCIG)

The first production of electrical energy with wind power was 1887 by Charles Brush in Cleveland, Ohio. The rated Power of the used dc-generator was 12kW and was designed to charge batteries. The induction machine was used at the first time in 1951. But, in wind power using squirrel-cage induction generators (see Fig. 7), must be operated at a constant speed, which is not favored at the varied wind speed application. However, SCIG drives have bulky construction, low efficiency, low reliability and need of maintenance, also the existing of slip ring, brush and three-stage gearbox increases the system mass and cost, also electrical and mechanical loss. Recently, squirrel-cage induction generators are dropping in this application. [10]

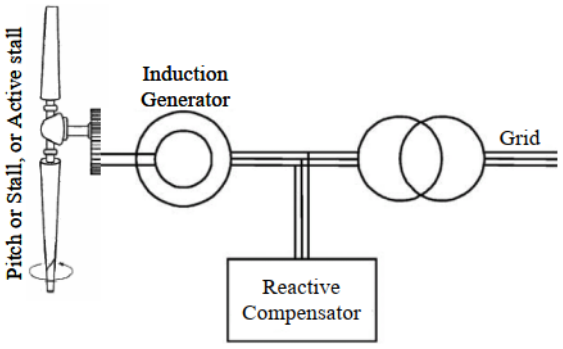

Figure 7 Scheme of a SCIG wind generating system

Typical torque speed curve of the machine is shown in Fig. 8. Hence, the rotor always rotates at a speed slightly lower than the synchronous speed. The difference between the synchronous speed Ns and the rotor speed Nr is termed as the slip of the motor. Thus, the slip (S) is given by:

$$S = \frac{N_s - N_r}{N_s} \quad (4)$$

When we couple this machine with a grid integrated wind turbine, initially it draws current from the grid as in case of a motor. The speed picks up and the rotation of the wind turbine causes the system to exceed the synchronous limit Ns .Thus, rotor moves faster than the rotating magnetic field. At speeds higher than Ns, the torque is negative as seen from Fig. 8. Thus, current flows in the opposite direction that is from the system to the grid. Thus, the machine functions as a generator when it is driven by an external prime mover, like the wind turbine in our case. Moreover, the development of rugged solid-state power semiconductors made it increasingly practical to introduce DF induction and synchronous generators drives that are mature to replace IG drive in wind power. [10]

For illustration, Fig. 9 shows industrial wind power induction generators.

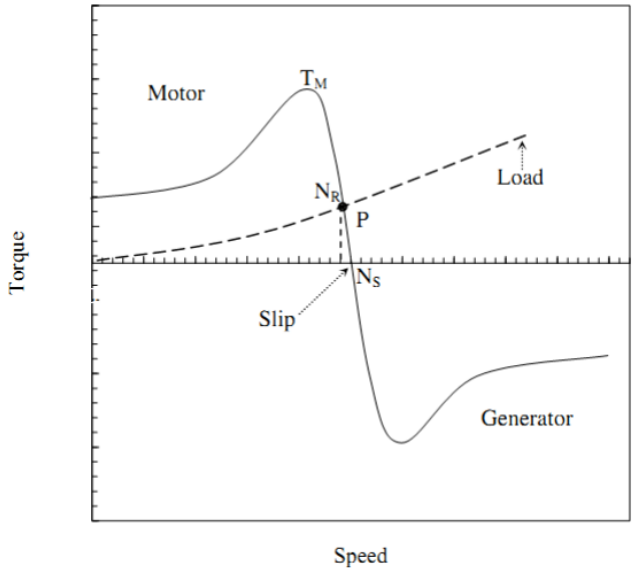

Figure 8 Characteristics of a typical induction machine

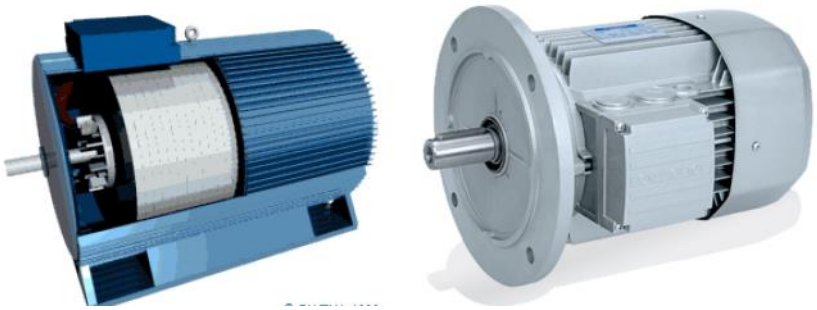

Figure 9 Industrial induction generator for wind turbine

1.3.2. Doubly-Fed Induction Generator (DFIG)

Today over 70% of the wind turbines are build up with Doubly-Fed Induction Generator (DFIG). Many manufacturers, such as Vestas, Gamesa, GE and Repower, have provided the wind turbine system with this concept Fig. 10. This system (Fig. 11) consists of a wind turbine with DFIG. This means that the stator is directly connected to the grid while the rotor winding is connected via slip rings to a converter. As also seen in the Fig. 12 the DFIG can operate both in motor and generator operation with a rotor speed range of ±Δw rmax around the synchronous speed, w1. The dynamic behavior model and their control system of the DFIG is considered in. [10]

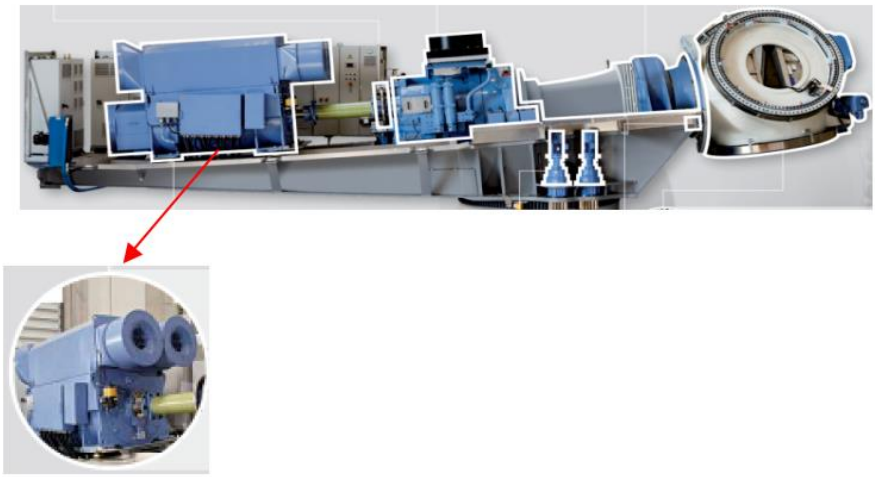

Figure 10 Industrial DFIG for wind turbine of the REpower manufacturer

Moreover, new types of generators which may change the configuration of the wind energy are being developed, where this new concept eliminates most of the mechanical parts, such as brush, slip ring and gearbox, that are considered drawbacks to this concept, as a result, reducing the mass and cost of the system and achieving high reliability and availability. Finally, it should be noticed that most research works tend to use the DFIGs in wind energy, as they have excellent performance [20-25]. Such as in [26] adjustable speed operation of the DFIG offers many advantages to reduce cost and has the potential to be built economically at power levels above 1.5 MW for off-shore applications.[10]

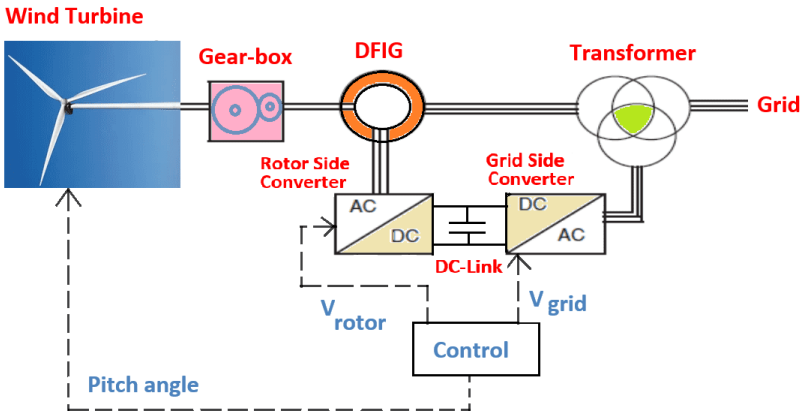

Figure 11 Scheme of a DFIG wind generating system

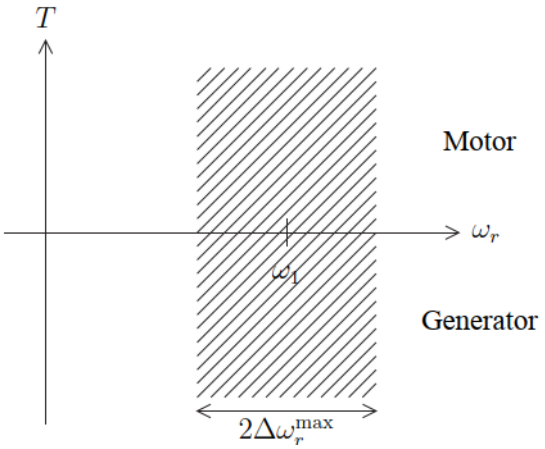

Figure 12 Torque-speed characteristic of a DFIG

1.3.3. Permanent Magnet Synchronous Generator (PMSG)

Permanent magnet synchronous generators (PMSG)s consists of a rotor and a three-phase stator similar to an induction generator are most capable of competing with induction generators for the wind power applications. In fact, they are adopted by well-known small wind turbine (Fig. 13). These generators have a number of advantages, which are:

(a) Simple and more effective configuration in the rotor with permanent magnet.

(b) Overall weight and volume significantly reduced for a given output power (high power density).

(c) Higher efficiency and self-excited.

(d) Heat efficiently dissipated to surroundings.

In the PMSG the air-gap flux density can be increased by increasing the thickness of the magnets. The air-gap flux density in the PMSG machine is approximated by the following equation:

$$B_m = B_r \frac{k_{leak}}{1 + \frac{\mu_r * g * k_{carter}}{h_m}} \quad (6)$$

Where:

hm : magnet thickness,

Br : residual flux density for the magnet. For NdFe35, it's 1.23 T.

g : minimum air-gap length,

μ_r : relative recoil permeability for the magnet. For NdFe35, it's 1.09981.

kleak: leakage factor. Typically in the range of 0.9 to 1.0 for surface-mounted PM machine.

Kcarter : Carter coefficient. Typically in the range of 1.0 to 1.1 for surface-mounted PM machine.

Although the PM machine can achieve a larger air-gap flux density and the stator bore diameter is smaller. Moreover, the advantage of the PM machine design is that it has a much higher efficiency (97 %) than the induction machine (85 %).

Due to their excellent performance especially, efficiency and reliability, the general trend in wind industry is to go for higher powers, which is especially relevant with harsh environment. it has become more and more popular during this year's. where several companies have been tried this concept:

Jeumont (0.75 MW), Vensys (1.5 MW), Leitner (1.5 MW), Harakosan (2 MW), Mitsubishi (2 MW), Siemens (3.6 MW), and TheSwitch (4.25 MW) [27]. In [31] work, there are summary of commercial wind turbine with synchronous machine (Large than 1MW). [10]

For illustration, Fig. 13 shows industrial PMSG 1650-6300 kW, 11-17 rpm.

Figure 13 Industrial permanent magnet synchronous generator

From analysis of the commercially available wind turbine generators, the elimination of the gearboxes and the power electronic converters will significantly increase the system reliability. The overall system efficiency will increase because the losses in the gearbox and power electronic converters are eliminated, it is concluded that direct drive, grid connected generators indicate a future trend in the wind generation. Finally, the reported results are promising, however, the requirement of PM materials restricts the applications of PMSG, either for high cost or potential to demagnetization in harsh environment. [10]

1.3.4. Switched Reluctance Generator (SRG)

An innovative Switched Reluctance Generators are gaining much interest and are recognized to have potential for wind power applications, the structure of a 6/4 SRG. These generators have the definite advantages of simple and rugged construction, fault-tolerant operation, simple control, and outstanding torque-speed characteristics (Fig. 14). SRG can inherently operate with extremely long constant power range. There are, however, several disadvantages, which for many applications outweigh the advantages. Among these disadvantages, acoustic noise generation, torque ripple, special converter topology, excessive bus current ripple, electromagnetic interference (EMI) noise generation. All of the above advantages as well as the disadvantages are quite critical for wind power applications. Nevertheless, SRG is a solution that is envisaged in the future for wind energy applications (Fig. 15). [10]

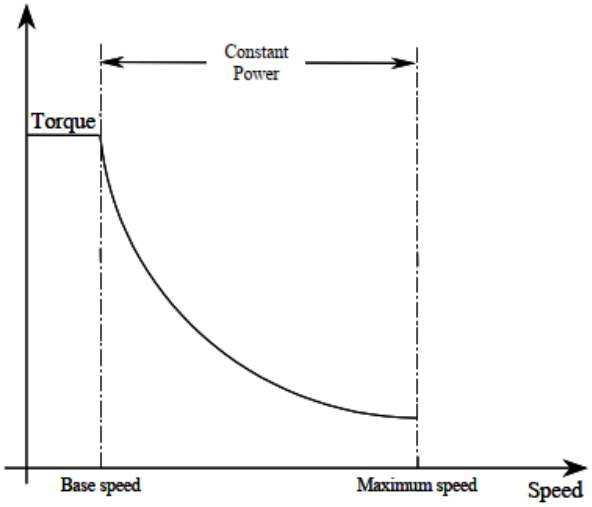

Figure 14 Typical torque-speed characteristic of a switched reluctance motor

Figure 15 Stator and rotor of the 20kW switched reluctance machine

2 Drives

2.1. Synchronous Generator

In a synchronous generator, a DC current is applied to the rotor winding producing a rotor magnetic field. The rotor is then turned by external means producing a rotating magnetic field, which induces a 3-phase voltage within the stator winding.

• Field windings are the windings producing the main magnetic field (rotor windings
• armature windings are the windings where the main voltage is induced (stator windings)

The rotor of a synchronous machine is a large electromagnet. The magnetic poles can be either salient (sticking out of rotor surface) or nonsalient construction.

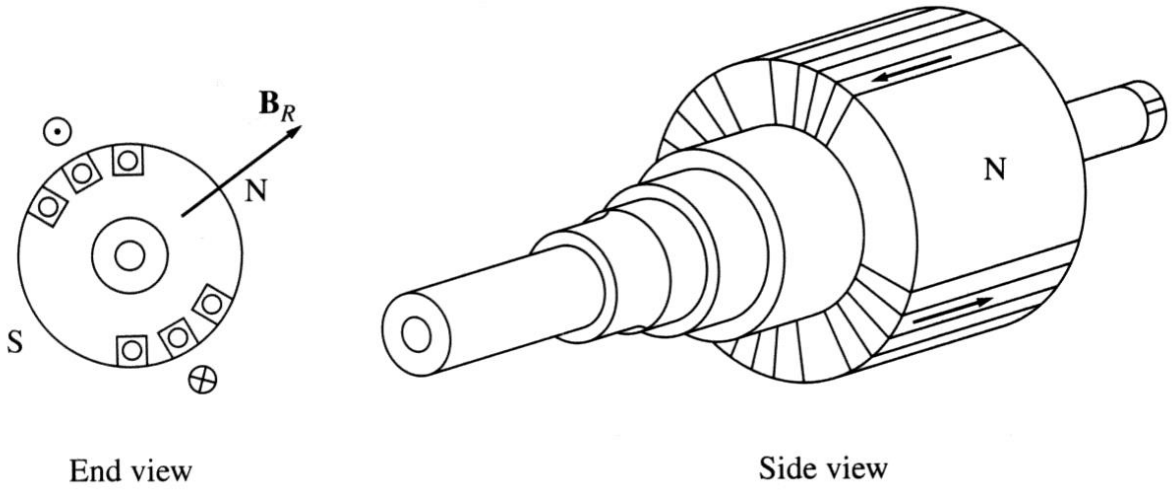

Figure 16 Synchronous generator Side View and End View

Synchronous generators can be classified as electrical excited synchronous generators (EESGs) and permanent magnet generators (PMGs)

2.1.1. Types of Excitation System for Synchronous Generators

Synchronous machine excitation systems can be classified into three major groups based on the power supply used as source of excitation. These are DC excitation, AC excitation and static excitation systems.

1) DC Excitation System:

This excitation system utilizes DC generators as source of excitation power. It also provides current to the rotor of synchronous machine through slip rings. The exciter can be driven by a motor or shaft of a generator. It can be either self-excited or separately excited. When it is separately excited, the exciter field current is supplied by a pilot exciter comprising of a permanent magnet generator. DC excitation systems represent early systems, spanning the years from the 1920s to the 1960s. They lost favor in the mid1960s and were superseded by ac excitation systems. [12]

2) AC Excitation Systems: These excitation systems utilize alternators as source of generator excitation power. Usually, the exciter is kept on the same shaft as the turbine generator. The AC output of the exciter is rectified by either controlled or diode rectifiers to produce the direct current which is needed for the generator field. The rectifiers can be stationary or rotating. AC excitation systems can take many forms depending on the rectifier arrangement, method of exciter output control, and source of excitation for the exciter. Currently, stationary and rotating AC rectifier systems are widely used in AC excitation systems. In stationary rectifiers, the DC output is fed to the field winding of the generator through the slip rings. On the other hand, in rotating rectifiers there is no need of slip rings and brushes. The DC supply is directly fed to the generator field as the armature of the exciter and rectifiers rotate with the generator field. Such systems are known as brush-less systems and were developed to avoid the problems with brushes when extremely high field currents are applied to large generators [13].

3) Static (ST) Excitation Systems: All the components of these systems are either static or stationary. Such systems directly provide synchronous generator field winding with excitation current by means of slip rings. Rectifiers in ST systems gain the power from generator through auxiliary windings or a step-down transformer. In such systems, generator is a source if power which means that the generator is self-excited. As the generator cannot produce any voltage without excitation voltage, the generator must have auxiliary power source to provide field current and energize the generator [14]. Station batteries are usually used as additional power sources and the process is known as field flashing. From the excitation power gain point of view the excitation systems can be further divided into independent and dependent excitation systems. The independent exciter is not connected to the grid. Thus, its excitation parameters have no direct relationship with grid parameters [14]. The dependent exciter utilizes either part of generator power or it is connected to the grid. Its excitation parameters are dependent on grip parameters

2.2. Permanent Magnet Synchronous Generator

The conventional asynchronous generator is generally connected to the turbine through a gear box. The permanent magnet synchronous generator (PMSG) can be coupled to turbine via a gear box or directly without a gearbox if the generator has a high number of poles. Due to increase of the power in the order of megawatts, today until 10MW, PMSG configuration necessitates an increasing of the size and the weight of the converters. Permanent magnet synchronous generators have the advantages of being robust in construction, very compact in size, not requiring an additional power supply for magnetic field excitation, and requiring less maintenance compared to conventional generators. In more, a variable speed wind energy conversion system including a PMSG offers advantages compared the constant speed approach, such as maximum power point tracking capability and reduced acoustic noise at lower wind speeds. [15]

PMS Generator has the following types,

- Radial Flux Permanent Magnet Generator
- Axial Flux Permanent Magnet Generator
- Transversal Flux Variable Speed Generator

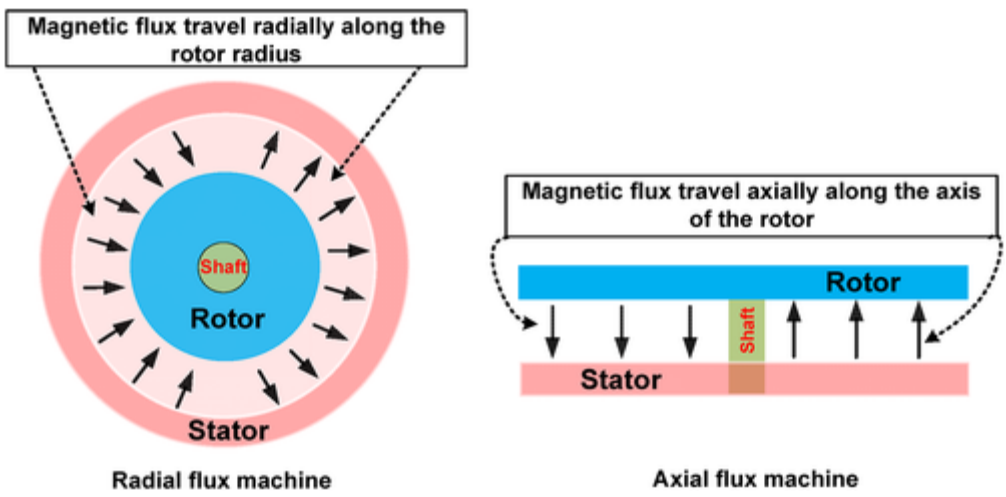

Figure 17 Radial Flux Machine and Axial Flux Machine

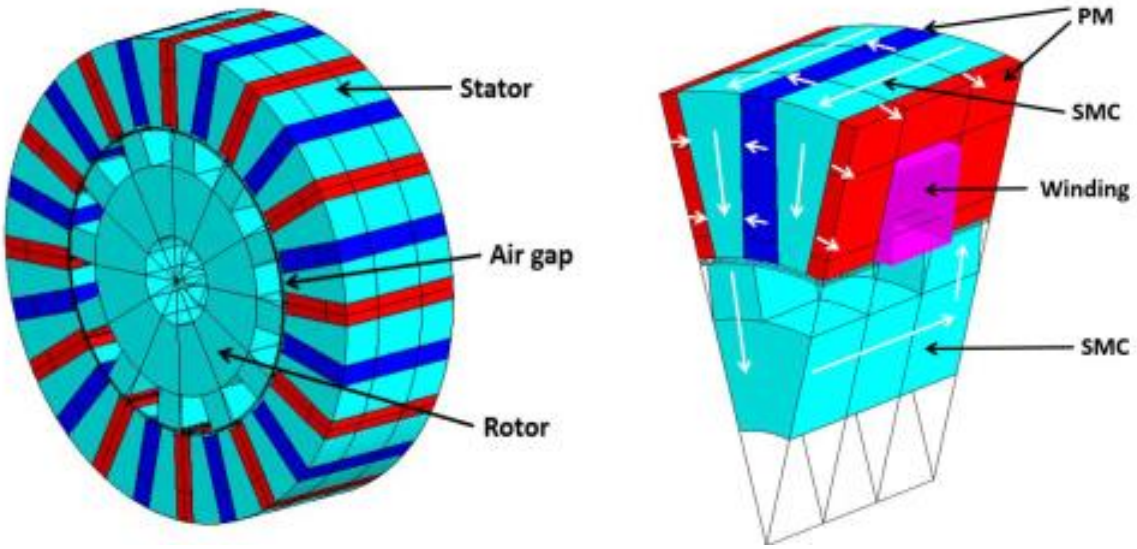

Figure 18 Stator PM - Transverse Flux Machine Topology and Flux Path (SMC* = Soft magnetic Composite)

2.2.1. Radial Flux PM Generator

A radial-flux permanent magnet (RFPM) direct drive generator derives its name from the radial orientation of its magnetic flux path, its permanent magnet excitation (PM) and its direct driven topology. In a radial flux machine, the magnetic flux lies perpendicular to the axis of rotation. The radial flux is produced by the permanent magnets present in this type of machine. These magnets replace the electromagnets produced by excited coils in other machines. One of the more popular alloys from which permanent magnets are manufactured, is known as neodymium-iron-boron (Nd2Fe14B). This is a type of rare earth magnet and is well known for its good strength to weight ratio. Rare earth magnets do however have some disadvantages such as high costs and material brittleness.

An alternative topology to the radial-flux machine is known as an axial-flux machine. In this case the magnetic flux path lies axially along the machine, parallel to the axis of rotation. A simplified illustration of these machines is shown in Fig. 5. In both of these topologies the rotors are made up of two interconnected steel disks which act as a housing and flux return path for the surface-mounted permanent magnets. An air-cored (iron-less) stator is located between the two opposing rotors. The stator consists of copper conductors embedded in a hardened epoxy resin. In this study the focus is on a RFPM generator type. [16]

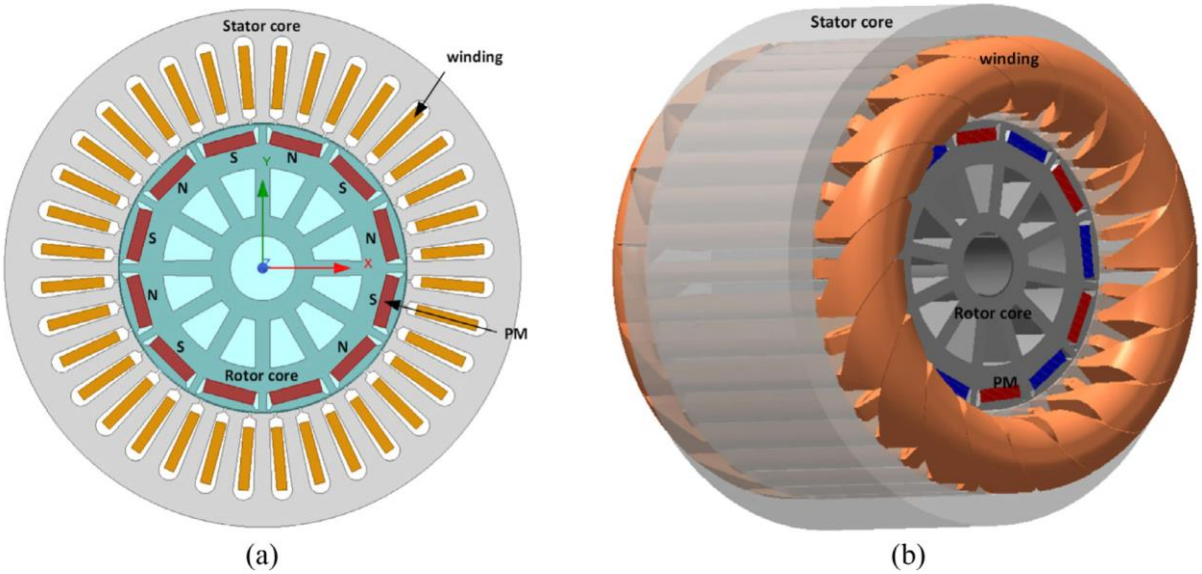

Figure 19 Radial flux PM generator structure, (a) 2D view, (b) 3D structure

2.2.2. Axial Flux PM Generator

In the recent studies, it has shown that the AFMs are very attractive and cost-effective alternatives for Radial Flux machines (RFMs) especially for applications such as small wind power system, aircrafts, compact engine generator sets, hybrid electric vehicles and direct battery charging.

Axial Flux Permanent Magnet (AFPM) machine size and shape are important features in applications where space is limited, so compatibility is crucial. Since PM machines are increasingly become very dominant machines with cost competitiveness of high energy PMs such as Neodymium Iron boron (Nd2Fe14). They are more efficient because field excitation losses are eliminated rotor loss reduction. Hence the generator efficiency is improved and high power density is achieved. AFPM machines have number of advantages over Radial Flux Permanent Magnet (RFPM) machines such as they have high power to weight ratio, high aspect ratio, reduced noise and vibration levels, adjustable air gaps and occupies less space etc., AFPM generators are most suitable than radial flux PM generators for small wind power applications.

The axial flux permanent magnet synchronous generator (AFPMSG) with high ratio of generator diameter to generator length is one of the appropriate choices in direct coupled wind turbine. Depending on design characteristics and according to the material used in the stator core, AFPMSGs are classified into two types: 1) iron-cored and 2) ironless generators. Compared with iron cored generators, ironless generators have the advantages of lightweight, high efficiency, no cogging torque, and simple construction. Moreover, in ironless generators, considering the negligible attraction force between the stator and the rotor, the structural mass of the generator is of

lightweight and provides reliable design for large generator diameters. However, because of the large effective length of the air gap, which requires a larger amount of PM material, in these generators, the active material cost is higher than iron-cored machines. In other words, the advantages of lower structural mass and higher generator diameter are obtained at the cost of higher active material price. [17]

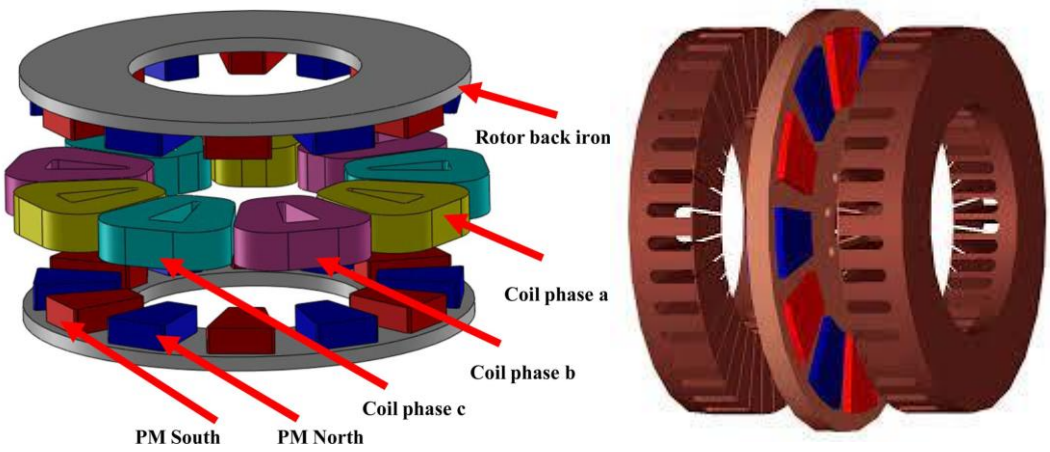

Figure 20 (Color online) Exploded view of the 3-D FEA model of

2.2.3. Transversal Flux Variable Speed Generator

The machine got the Transverse Flux name because its flux path is not confined to any single plain but is three-dimensional in nature. However, the three-dimensional flux path is only a characteristic feature of TFM, but not the fundamental difference that sets TFM apart from radial flux or axial flux machines. TFM's distinguishing identity lies in its monopolar concentrated ring winding. [18]

Figure 21 shows one phase module of the TFM that is distinguished by its concentrated ring winding. Segmented stator cores, usually C-shaped, are aligned circumferentially following the shape of the winding. The monopolar phase winding sits in the common slot of the stator poles, such that all the winding conductors are magnetically linked with all the stator poles. In this case, the shape of the stator poles modulates the winding MMF to create north and south magnetic poles at either end of the C-cores.

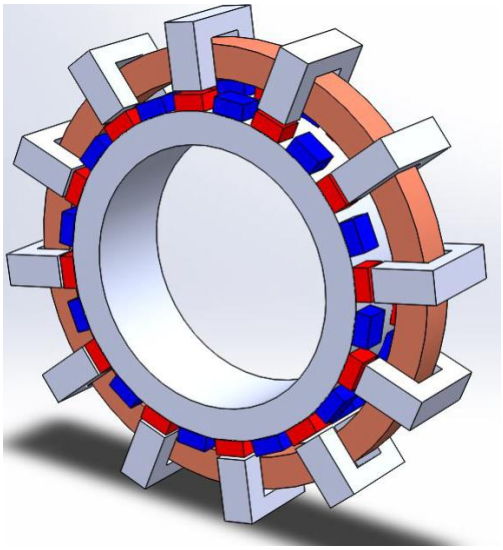

Figure 21 Transverse Flux Machine

2.3. Comparison Between Axial Flux and Radial Flux Machines

The most important consideration for a machine's performance is its volumetric power density and efficiency. AFPM machines have better volumetric power density and efficiency than RFPM machines. The calculation of the efficiencies includes the ohmic losses and the iron losses in stator and rotor. The friction losses and additional losses like eddy-current losses in the magnets were neglected.

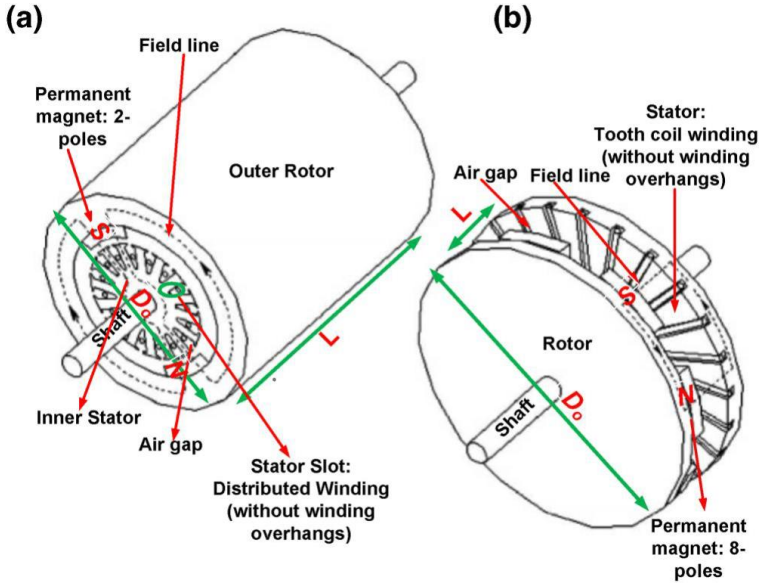

Figure 22 The structural difference between axial- and radial-flux

A comparison is made between AFPM and RFPM machines for a fixed pole number of motor, wherein higher torque density was found with AFPM machines. Moreover, AFPM machines can be designed to have a higher power-to-weight ratio resulting in less core material. The torque density variation with an aspect ratio (k) for different pole numbers is shown in Figure 22 for RFPM and AFPM machines. From a comparative view, it is apparent that for the same pole number, the AFPM machine delivers almost the same torque density with a lower aspect ratio. For example, to provide a torque density of 6.5 Nm/kg with 20 poles, the AFPM requires an aspect ratio ($k < 0.2$) considerably lower than that needed for an RFPM ($k > 0.35$). For aspect ratio $k > 1$, RFPM needs a long motor shaft, which eventually increases its weight resulting in lower torque density. In addition, the AFPM has planar and easily adjustable air gaps. The noise and vibration levels of AFPM machines are less than those of the RFPM machines. Also, the direction of the main air-gap flux can be varied, and many discrete topologies can be derived. These benefits present the AFPMs with certain advantages over conventional RFPMs in various applications. [19]

3 Design Considerations of DDPM Machines

3.1. Mechanical Structure of DDPM Generators

The rotor of a direct-drive generator for a wind turbine is directly connected to the rotor blades. Thus, the direct-drive generator operates at low speed. When the wind turbine is scaled up, the rotational speed is decreased further because the tip speed is kept constant. In order to scale up the power of the direct-drive generator P, the increase in torque T must be thus inversely proportional to the decrease of the mechanical angular speed ωm as given in (7)

$$P = T\omega_m \quad (7)$$

The torque of the generator T is proportional to the tangential force F and the air gap diameter Dg. The tangential force F can be defined as the product of the tangential force density Fd and the air gap area Ag. Thus, the generator power P can be also defined as (8)

$$P = \frac{\pi}{2} F_d D_g^2 l_s \omega_m \quad (8)$$

where ls is the axial length of the generator.

The torque is proportional to the air gap diameter squared, thus the direct-drive generator is generally built with a larger diameter to produce higher torque. Larger air gap diameter results in an increase of materials to construct the generator against the normal stress due to the flux density between the rotor and stator. Therefore, the direct-drive generator that operates at low speed has a high torque rating, a large diameter, a large mass and a high cost. The most common mechanical structure for electric machines supports the rotor shaft simply between two bearings housed in the stator frame as illustrated in Fig 23

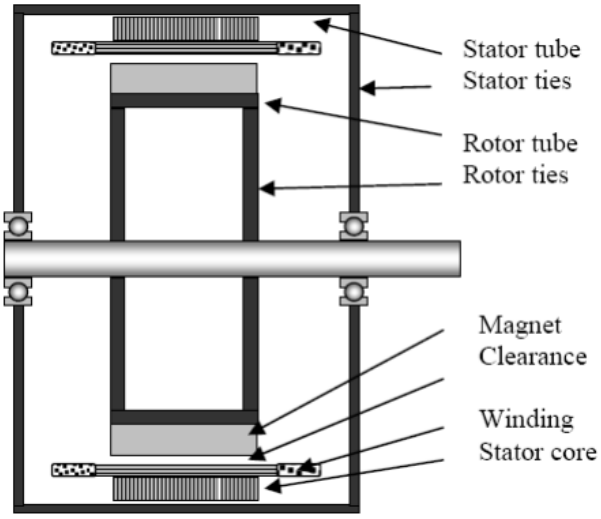

Figure 23 The traditional mechanical structure of electric machines [20]

Direct-drive wind generators have meanwhile used different mechanical structures as Fig. 24. An inner rotor with a double bearing concept, the conventional concept for wind turbines, is illustrated in Fig.24(a). Fig. 24(b) depicts a concept with an inner rotor with a single bearing, which is often used to save on bearing costs. A concept with an outer rotor with a double bearing is shown in Fig. 24(c).

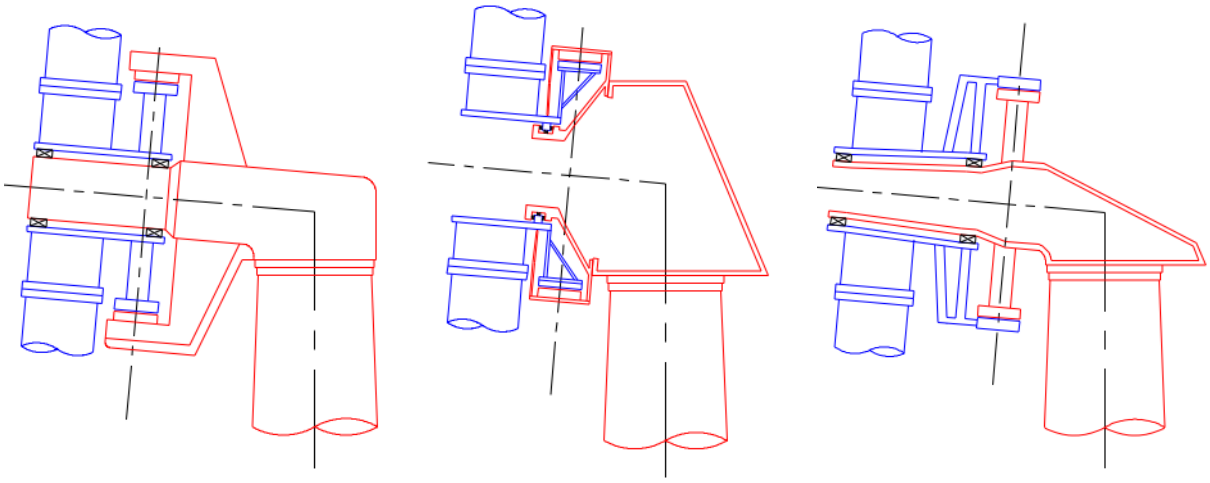

(a) Inner rotor with double bearings *(b) Inner rotor with single bearing* *(c) Outer rotor with double bearing*

Figure 24 Different mechanical structures of direct-drive wind generators [20]

3.1.1. Conventional Structure

Traditionally the rotor of generator is connected to a shaft mounted on bearings that enable the rotation in the stator as shown in Fig. 23 The structure of Fig. 24(a) is widely

used on the wind turbine market by Enercon GmbH, whose world market share was about 10 % in 2008. Fig.25 depicts the generator structure of Enercon's E-112 model. The generator is an electrically excited direct-drive synchronous generator, whose total mass and diameter are about 220 tonnes and 12 m, respectively [22].

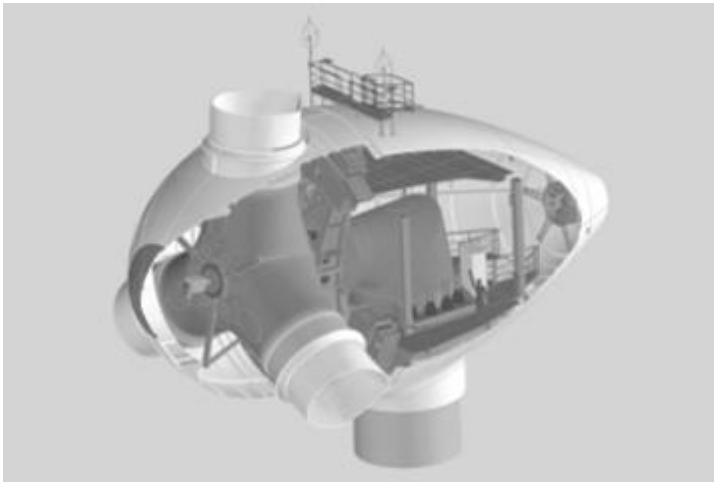

Figure 25 Structure of 4.5 MW electrically excited direct-drive synchronous generator [23]

The the mass minimization of the permanent magnet excited direct-drive generator with traditional mechanical structure was discussed for different power ratings: 2, 3 and 5 MW. In order to minimize the total mass of the generator, the ratio of axial length to air gap diameter Krad has been optimized. Fig. 26 depicts the structure of the rotor. Fig. 27 depicts the total mass of the generator as a function of the ratio Krad. The Krad of 2, 3 and 5 MW generators chosen as the optimum value are 0.2, 0.22, and 0.27 respectively. It is also shown that the structural mass of large direct-drive wind generator is dominant in the total mass when scaling up the power rating [24]

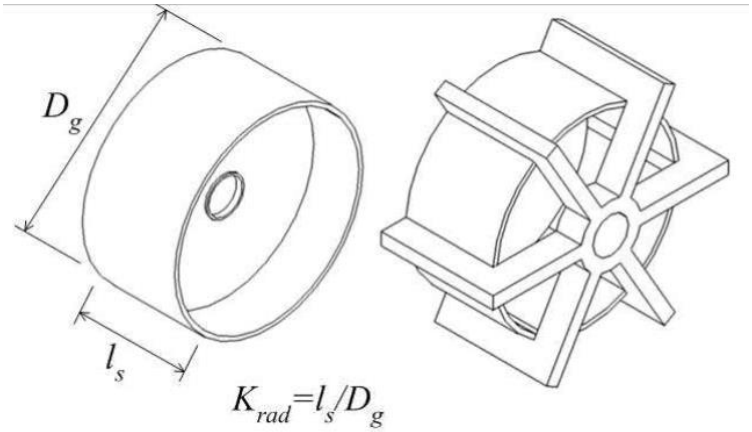

Figure 26 Structure of the rotor and stator for structural optimization [24]

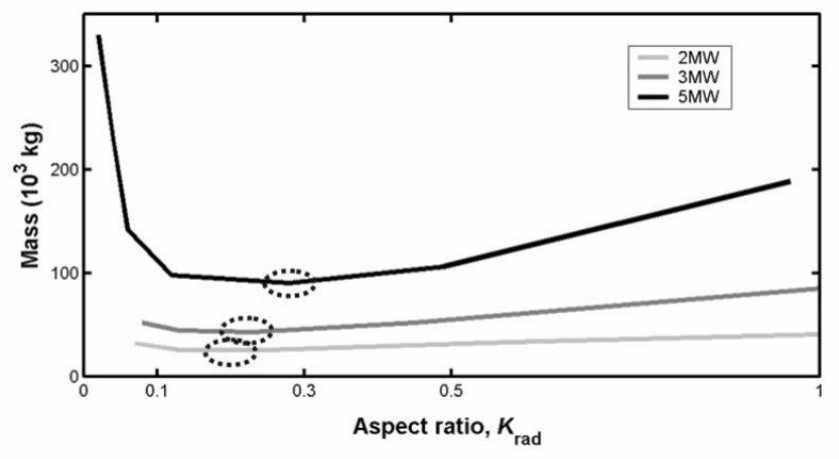

Figure 27 Total mass of 2, 3 and 5 MW PMSG DD as a function of the ratio, Krad [24]

3.1.2. Lightweight structure

A single-bearing structure of Fig. 24(b) has been used by Zephyros B.V., currently STX Windpower B.V. [25]. A cone-shaped hollow structure with a single bearing is used for the generator instead of a traditional main shaft with two bearings as illustrated in Fig. 28. The diameter of the generator is smaller than the diameter of the conventional electrically excited synchronous generator. In this structure, the mechanical load path seems shorter than the traditional structure with a main shaft. Therefore, the structural mass of this structure can be smaller than the mass of the traditional structure.

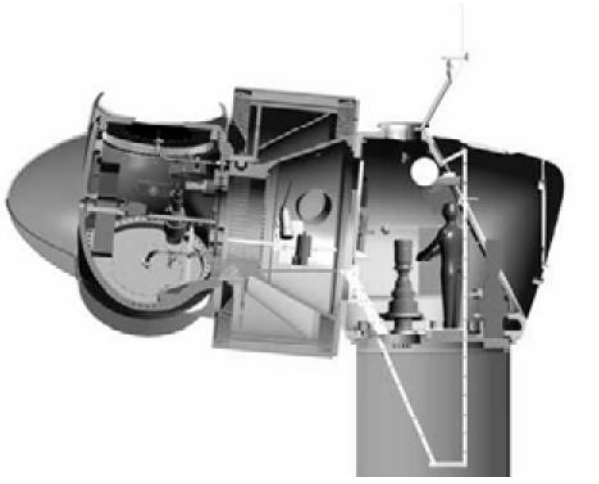

Figure 28 Structure of 1.5 MW permanent magnet direct-drive synchronous generator with a single bearing [25]

A new direct-drive generator for wind turbines has been proposed in [22]. The fundamental idea of the machine - the NewGen (see Fig. 4-2-7) is to reduce the stiffness demand by removing the load path from the rotor, the shaft and the stator by putting the bearings close to the air gap.

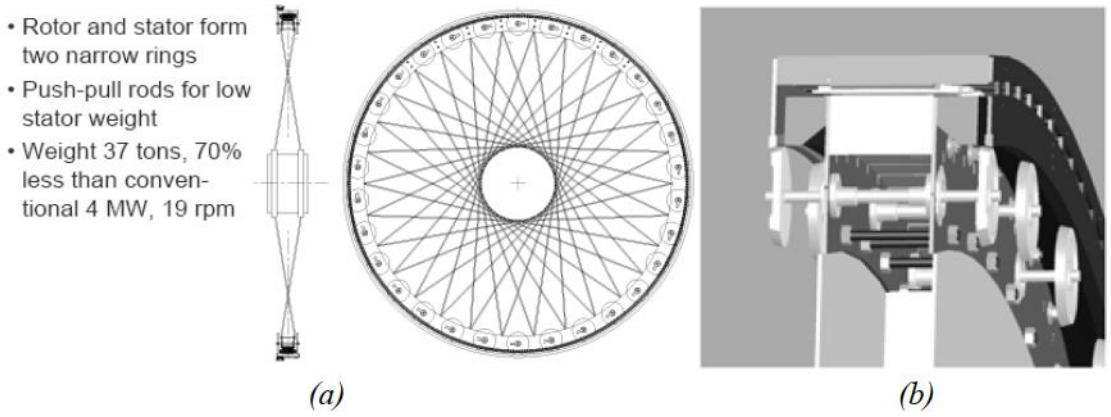

Figure 29 New Generator [22]

3.2. Thermal behaviour of DDPM

A permanent magnet motor has been developed rapidly due to its advantages such as high efficiency and excellent speed control performance. Meanwhile, the goal of obtaining greater output power and smaller size is always the dream of motor practitioners. That means that more and more heat accumulates in a smaller and smaller space, and the resulting temperature rise has a significant impact on motor winding insulation and permanent magnet demagnetization. Therefore, it is necessary to calculate the temperature of the motor during design to ensure that the motor runs at a safe temperature. [26]

For motors with different structures, the steady temperature rise of the motor is determined by the heat dissipation capacity. For AFPM and RFPM, the heat generated inside the motor is emitted to the external environment through the casing and water channel. The motor output is same under the same size. When the motor tends to be miniaturized, the steady temperature rise of the motor has important reference for the choice of the motor structure. ETNM of the motor is established by the existing thermal resistance model. Furthermore, the influences of parameters on the steady state temperature rise of the two kinds of motors are studied here. [26]

3.2.1. Equivalent Thermal Network Model

To build to ETNM, the following assumptions are necessary.

• The temperature distribution of motor is symmetric along the circumferential direction. For AFPM, the temperature distribution on both sides of the disk is also symmetric.

• The temperature at each air node of motor is same.

- The influence of radial heat dissipation on temperature distribution is ignored.
- The cooling water of motor is isothermal.

Namely, only one temperature node of cooling water temperature is used. The objects analyzed are an AFPM with double-stator single-rotor and a RFPM with inner rotor, the main structures of which include water jacket, end cover, stator yoke, stator tooth, winding, permanent magnet, rotor, bearing, etc. The node distributions of ETNM are shown in Fig 30 and Table I. [26]

$$\Delta T = G^{-1} P \tag{9}$$

$$G = \begin{bmatrix} \sum_{i=1}^{n} \frac{1}{R_{1,i}} & -\frac{1}{R_{1,2}} & \cdots & -\frac{1}{R_{1,n}} \\ -\frac{1}{R_{2,1}} & \sum_{i=1}^{n} \frac{1}{R_{2,i}} & \cdots & -\frac{1}{R_{2,n}} \\ \vdots & \vdots & \ddots & \vdots \\ -\frac{1}{R_{n,1}} & -\frac{1}{R_{n,2}} & \cdots & \sum_{i=1}^{n} \frac{1}{R_{n,i}} \end{bmatrix} \tag{10}$$

where P is node thermal source, ΔT is node temperature rise, G is a n×n thermal conductivity matrix obtained by the thermal resistances of different motor parts, in which the diagonal element is the sum of the thermal conductivity connected with the corresponding node and the off-diagonal element is the thermal conductivity between nodes i and j.

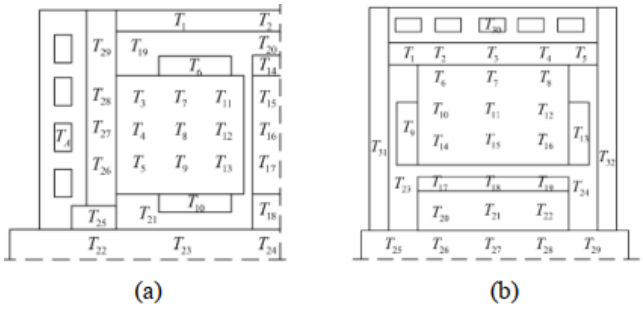

(a) (b)

Figure 30 Nodes distribution diagram of (a) AFPM, (b) RFPM. [26]

Table 1. NODE DISCRIPTION [26]

Component	AFPM	RFPM
Housing	1~2	1~5
Stator yoke	3~5	6~8
Winding	6~10	6~10
Stator teeth	11~13	14~16
Rotor	14~18	20~22
Permanent magnet	15~17	17~19
Motor internal air	19~21	23~24
Shaft	22~25	25~29
End cover	26~29	31~32
Water jacket	A	33

3.2.2. Equivalent Thermal Resistance Model

Heat transfer in the motor mainly includes heat conduction, convection heat dissipation and their synthesis.

A. Heat Conduction

Heat conduction can be expressed as follows by the Fourier law

$$q_c = -\lambda grad T \tag{11}$$

where qc is intensity of the heat transfer, λ is the thermal conductivity of conducting medium, gradT is temperature gradient.

The thermal resistance of heat conduction of a tube wall is

$$R_c = \frac{T_1 - T_2}{q_c} = \frac{1}{2\lambda\pi l}\ln\frac{r_2}{r_1} \tag{12}$$

where r1 and r2 are radii of inner and outer walls respectively, T1 and T2 are temperatures of inner and outer wall respectively, l is wall length, as shown in Fig. 31.

For a general rectangular component as shown in Fig.32 the conduction thermal resistance is

$$R_c = \frac{T_1 - T_2}{q_c} = \frac{l}{ab\lambda} \tag{13}$$

$$G_c = \frac{1}{R_c} \tag{14}$$

B. Equivalent Winding Model

Different winding forms have different thermal resistance equivalent models

$$R_{s1} = \frac{C_i}{\lambda_i} + \frac{1}{4}\left[\frac{b_s(1-\sqrt{S_f})}{\lambda_L}K_L + \frac{b_s(1-\sqrt{S_f})}{\lambda_a}\times(1-K_L) + \frac{h_{d1}}{\lambda_d}\frac{b_s\sqrt{S_f}}{d_1}\right] \tag{15}$$

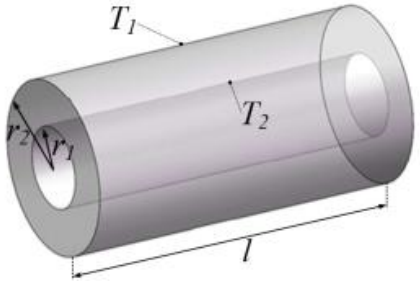

Figure 31 General cylindrical component

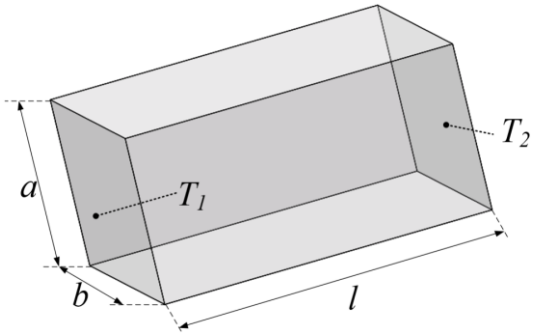

Figure 32 General rectangular component

where Ci is thickness of slot insulating varnish, λi is thermal conductivity of insulation varnish, λd is thermal conductivity of wire coating, bs is slot width, KL is filling coefficient of varnish.

C. Equivalent Winding Model

According to Newton's law, the heat of convective heat dissipation is proportional to the area of solid heat dissipation and the temperature difference of convection, it can be calculated as follows

$$q_h = hS\left(T_z - T_f\right) \tag{16}$$

where qh the heat flow intensity, h is coefficient of convective heat dissipation, Ts is solid temperature.

The resistance of convention heat dissipation is

$$R_h = \frac{1}{hS} \tag{17}$$

$$G_h = \frac{1}{R_h} \tag{18}$$

Heat dissipation coefficient has great influence on convection heat dissipation. Through comparative analysis, we determine the following partial convection heat dissipation coefficient.

(1) Air Gap

Heat exchange is carried out in the stator rotor through the air gap, and its convective heat dissipation coefficient can be calculated by Reynolds number and corresponding Taylor number and Nussel number [27]

$$\mathrm{Re}_\delta = \frac{v_r g}{\mu_{air}} \tag{19}$$

$$Ta = \frac{\mathrm{Re}_\delta^2 g}{r} \tag{20}$$

$$Nu = \begin{cases} 2, & \text{if} \quad Ta < 1700 \\ 0.128 Ta^{0.367}, & \text{if} \quad 1700 < Ta < 10^4 \\ 0.409 Ta^{0.241}, & \text{if} \quad 10^4 < Ta < 10^7 \end{cases} \tag{21}$$

$$h_{air} = \frac{Nu \cdot \lambda_{air}}{g} \tag{22}$$

where g is air gap length, vr is rotor circumferential velocity, μair is air dynamic viscosity, Nu is Nussel number, Re is Reynolds number, and hair is air gap heat dissipation coefficient.

(2) Watercourse

$$\mathrm{Pr} = \frac{\mu_w \rho_w C_w}{\lambda_w} \tag{23}$$

$$\mathrm{Re} = \frac{v_w \Delta W}{\mu_w} \tag{24}$$

$$Nu = 0.023\,\mathrm{Re}^{0.8}\,\mathrm{Pr}^{0.4} \tag{25}$$

$$h_w = \frac{\lambda_w Nu}{\Delta W} \tag{26}$$

where μw is fluid flow viscosity, ρw is fluid density , Cw is specific heat capacity of fluid, vw is fluid velocity, Pr is the Prandtl number, ΔW is the hydraulic of the watercourse, hw is heat dissipation of watercourse

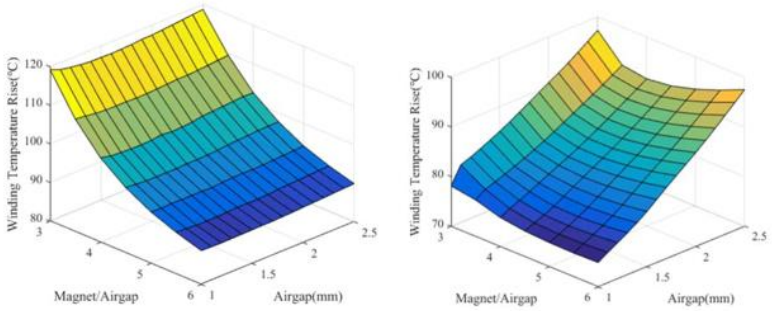

Figure 33 The influence of permanent magnet thickness and polar arc coefficient on the average temperature rise of winding of (a) AFPM, (b) RFPM

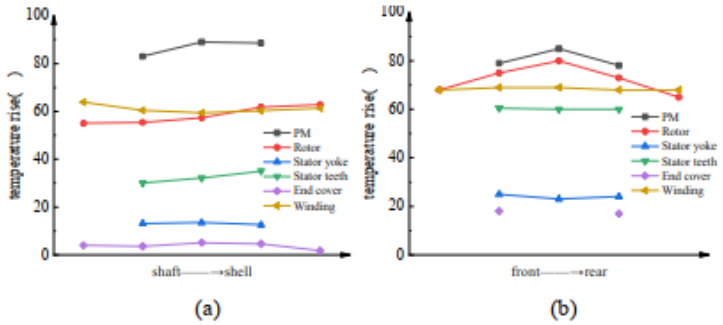

Figure 34 Temperature-rise distribution of (a) AFPM, (b) RFPM

The influences of main design parameters such as air gap length and polar arc coefficient on the temperatures of different parts of AFPM and RFPM under rated load are studied, and the temperature rise distribution characteristics of AFPM and RFPM are compared. The results show that the influences of the same parameter on the temperature rise of motors with different magnetic flux structures are different. Furthermore, the essence of temperature rise change is the changes of heat source and thermal resistance. Both heat source and thermal resistance are affected by most of the parameters. [27]

3.3. Electromagnetic Design for DDPM

There are many important aspects of design to consider, and it is not easy to define or derive an optimum design in some simple closed forms. But, it is possible to make an optimum choice of machine construction, just keeping in mind the requirement to achieve sufficient output power from given dimensions, and to be able to predict performance at variable load. Because of the possible non-linearity, an iterative numerical method is used to determine the operating point of the magnet. The approaches involve discretization of the magnetic circuit and integration of loop flux path. Repeated calculation and optimised device aim at obtaining possible high output, good performance and low cost of the product.

The determination of the dynamic operation point of the magnet needs to find the resultant magnetic potential differences along the discrete sections of the flux path. The leakage flux resulting from the polarisation of the magnets affects the density in critical parts of the magnetic circuit and main flux. It is necessary to set up a simultaneous equation relating to the balance between m.m.f. and reluctance drops throughout the entire path. Applying Maxwell's equation in this machine, an equation for electromagnet calculation can be obtained,

$$\int_m Hdl - \int_s Hdl - \int_r Hdl - \int_g Hdl = \int_\Omega Jd\Omega \qquad (27)$$

Where, subscript m, s, r. and g express the integral paths across magnet, stator, rotor, and air gap respectively as shown in Fig 35. The R is the integral area embraced by the entire integral path and J the current density. The first and the last integrals in the equation (27) are respectively referred to m.m.f. of magnet and armature reaction. The integral path is also shown in Fig. 35. In the subsequent calculation and analysis, a simulation is supposed that a smooth stator replaces the slotted stator. Carter's coefficient is used to modify the air gap such that a larger air gap length than the actual one is used in the calculation. [28]

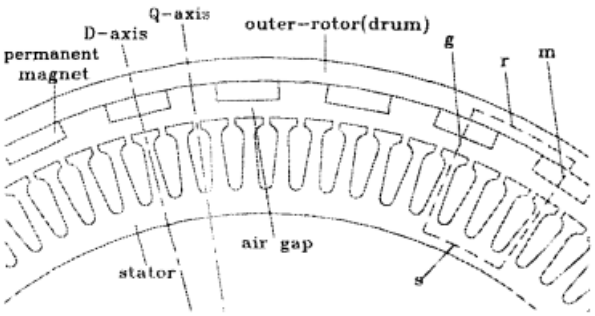

Figure 35 Cross section of PM generator

3.3.1. Static Operation

Referring to the open-circuit operation of this permanent magnet generator, the flux in the air gap, linking the stator winding, is produced solely by the magnets and induces an open-circuit voltage E, in the armature, which corresponds to the open-circuit operating point of the magnet. To plot this point on the B/H characteristics, it is assumed that the demagnetisation curve is a stabilised one with a single valued relationship. Namely, the demagnetisation within the range of operation is reversible. Normally, permanent magnetic materials have a linear curve for operation in the second quadrant on B/H characteristic. This certainly applies to the Nd-Fe-B magnet. Although magnetic field intensity H is negative in the second and third quadrants, it is preferred to regard H as a positive value for convenient calculation. The B/H line can be defined as: [29]

$$B = -\mu' H + B_r \tag{28}$$

The slope is,

$$-\mu' = B_r / H_c \tag{29}$$

Where -μ' is the apparent permeability, B, the residual flux density and H, the coercive field intensity. But this applies to magnetic materials and not to the magnet itself. So far as a magnet with given geometry goes, i t is more convenient to use Φ/F characteristic. This can be directly obtained from B/H characteristic through the following relations,

$$\Phi = BA_m \text{ and } F = Hh_m \tag{30}$$

Where Am, and hm are the face area and height of magnet. This demagnetizing characteristic is linear with intercepts equal to Φr = BrAr, and Fc= Hchm

$$\Phi = -(\Phi_r / F_c)F + \Phi_r \tag{31}$$

The quantity Φr/Fr, is the demagnetising curve of the magnet. The integral paths are selected both for the main flux and leakage flux, and there should be a balance between the reluctance drop and the m.m.f. The total flux Φm, supplied by permanent magnets, equals the sum of main flux Φ_Σ and leakage flux Φσ, distributed along the flux path. It is expressed as

$$\begin{aligned} \Phi_m &= \Phi_\Sigma + \Phi_\sigma \\ &= F_m/(R_g+R_s+R_r) + F_m\Lambda_\sigma \\ &= F_m\Lambda_\Sigma + F_m\Lambda_\sigma \end{aligned} \tag{32}$$

Where, the Ax and Aσ are the permeance for the main flux and leakage flux. The main flux path within a pair of poles consists of rotor yoke, two magnets, two sections of air gap, stator teeth and yoke. As the designed flux density in the teeth is below saturated level, the permeability H. in steel is far greater than unity. Comparing with the magnetic potential difference across the air gap, the reluctance drops in the stator and rotor are only a small part. The resultant permeance Aex of the entire magnetic circuit can be expressed as

$$\Lambda_{ex} = \Phi/F_m = \Lambda_{\Sigma} + \Lambda_{\sigma} \qquad (33)$$

The Aex is the resultant permeance of no-load magnetic circuit and represents the external magnetic effect to the magnet. The operating point corresponding to the open-circuit load is plotted at the intersection 0′ of no-load line with the demagnetising curve, as shown in Fig. 36. Its coordinate Φm, on Φ-axis represents the total flux coming out from a magnet face. The angle of the no-load line is

$$\alpha'_{ex} = \arctan \Lambda_{ex} \qquad (34)$$

The two lines with slope of main permeance AΣ and leakage permeance Aσ, are also shown in the Fig. 36. The operating point can be found by directly applying the iterative method on the Φ/F characteristic. As the flux Φ is one of the most concemed parameters in magnetic design, it is convenient to directly determine the operating point by using magnetic Φ/F characteristic and permeance lines. However, it is explicit to use the B/H characteristic to analyse the magnetic field of machines without considering the effect of different sized magnets, and features of magnets made of various materials in a certain magnetic circuit. In the B/H characteristic, a relative parameter p_{ex} is used to replace Aex

$$p_{ex} = \Lambda_{ex} (h_m/S_m) \qquad (35)$$

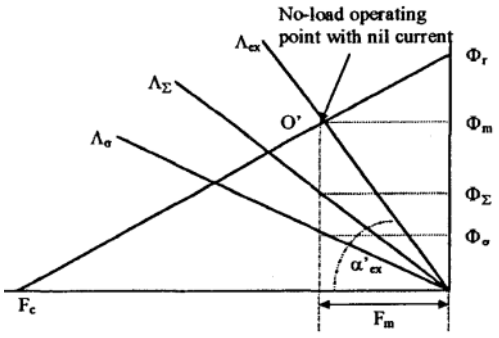

Figure 36 No-load operating point of magnet

A similar curve is shown in Fig. 37. The pex is the permeability line of no-load operation, representing the affection of external magnetic circuit at no-load operation. The operating point corresponding to the open-circuit load is 0′. Its coordinate Bm, on B-axis represents the flux density yielded from magnet face. The angle of the no-load line is

$$\alpha_{ex} = \arctan p_{ex} \tag{36}$$

3.3.2. Dynamic Operation

With the current flowing through the winding, the magnetic flux of the generator is significantly affected by an external magnetomotive force which is caused by armature reaction, and its operating point varies with the applied external magnetic field intensity. The corresponding position of dynamic operation depends on both the direction and amplitude of the armature reaction. The air gap field, set up by the stator armature current, possesses direct-axis and quadrature-axis components, which bears a close relation to the inductances Ld and Lq.

The flux across a magnet face either adds to or subtracts from the magnet flux, depending on the direction of the direct-axis current which is defined by the angle 8 between E, and load current I. A positive sign for Id means a magnetizing action and a negative sign a demagnetizing action with respect to the field direction of magnets. In the case of this generator, more attention is paid to the latter. The magnetic field intensity caused by the direct-axis armature current can be deduced from the field theory of electrical machine. It is known that the amplitude of magnetomotive force produced by the three-phase D-axis armature current under one pole is:

$$F_{ad} = \frac{3}{\pi}\frac{2\sqrt{2}W_p k_w}{p} I\sin\theta = 2.7\frac{W_p k_w}{p} I\sin\theta \tag{37}$$

To be used for plotting the load operating point directly on the B/H characteristic, equation (37) should be divided by k

$$H_{ad} = F_{ad}/h_m = 2.7\frac{W_p k_w}{p h_m} I\sin\theta \tag{38}$$

To determine the operating point on the B/H characteristic, the field strength Had caused by armature reaction can be directly added to the static operation characteristic. The no-load line is shifted along the H-axis for a value of Had and intersects the magnetic demagnetizing curve at point L shown in Fig.37. L is the normal operating point of the magnet, with the load. The corresponding coordinate Bad on the B-axis is the resultant flux density.

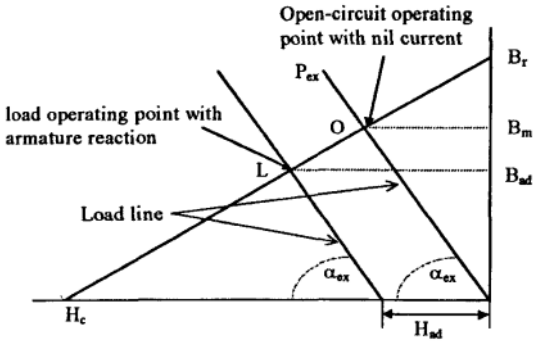

Figure 37 Load operating point of magnet

3.3.3. Machine Performance

To investigate the performance of this type of generator, a prototype machine was built with an intention to deliver an output power of 20 kW at a supposed rotational speed of 170 rpm. A comparison of the performance is made between the results of the computation and measurement.

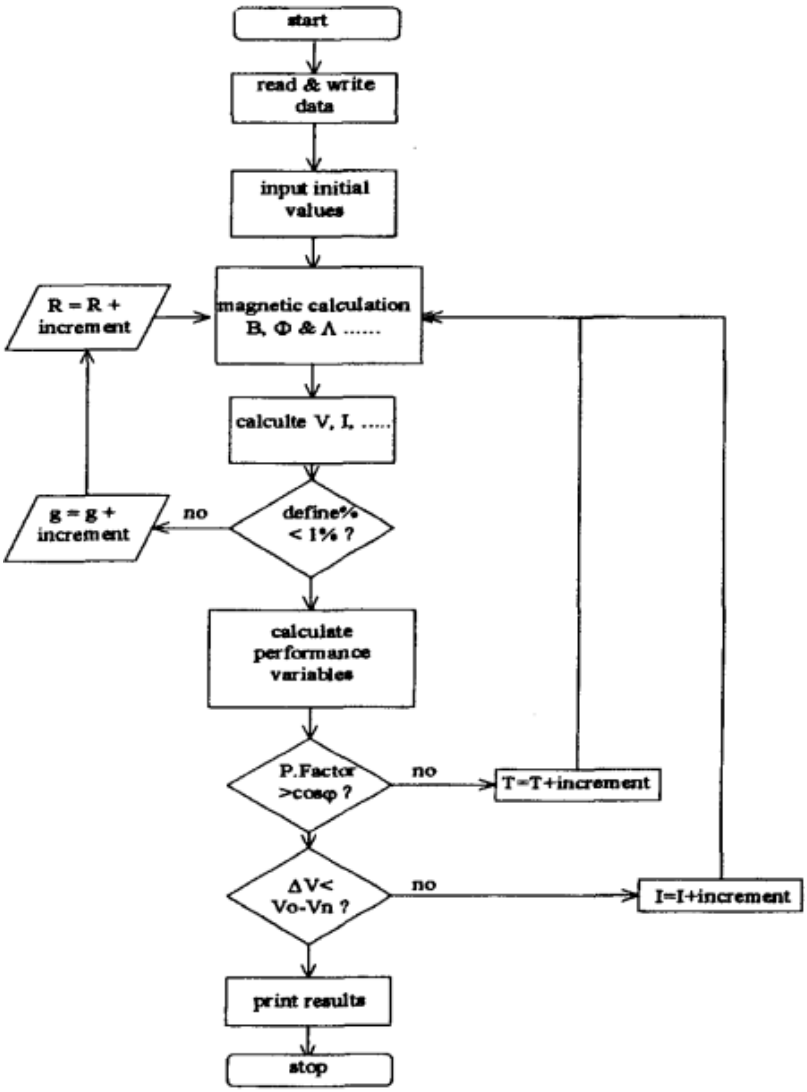

Figure 38 Computer program flow chart [28]

(1) Open-Circuit Characteristics

The open-circuit test was made under various rotational speeds. Fig.39 shows output RMS line to line voltages from computation and measurement. The test results show that the output terminal EMF is linearly proportional to the rotational speed, and the machine is therefore operated at the unsaturated region, which was intended in the design.

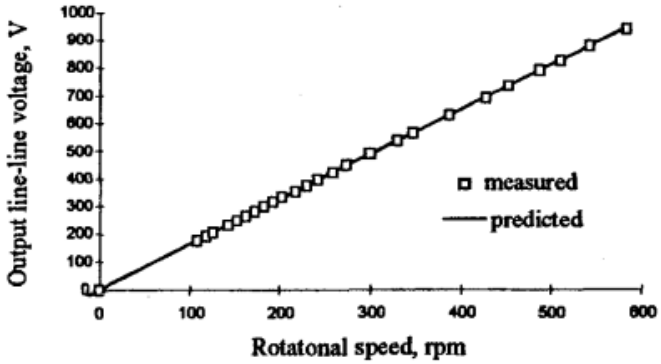

Figure 39 Open-circuit characteristics of the PM generator [28]

(2) Performance of Load test

The prototype generator was tested with a symmetrical 3- phase, variable resistive load. Armature reaction was found to have a significant influence on the output characteristics of the machine. At no-load test, the output voltage presented a non-sinusoidal waveform. However, as the load current increased, especially in the region above 13 A, this waveform became more sinusoidal. Except fundamental, the harmonic content of the original waveform was greatly reduced. The larger the load current, the higher the quality of the output sine wave. Except fundamental, other harmonics were remarkably weakened as the load current increased.

It was the expected behavior that the generator is capable of producing a good sine wave over wide loading range. This trend was promoted by increasing load current at two cases that either the load resistance was reduced while maintaining a constant speed, or the frequency was increased at the constant load resistance. In each of the cases, the inductive component of load current was enhanced. This changing tendency could be easily detected through the tests. [28]

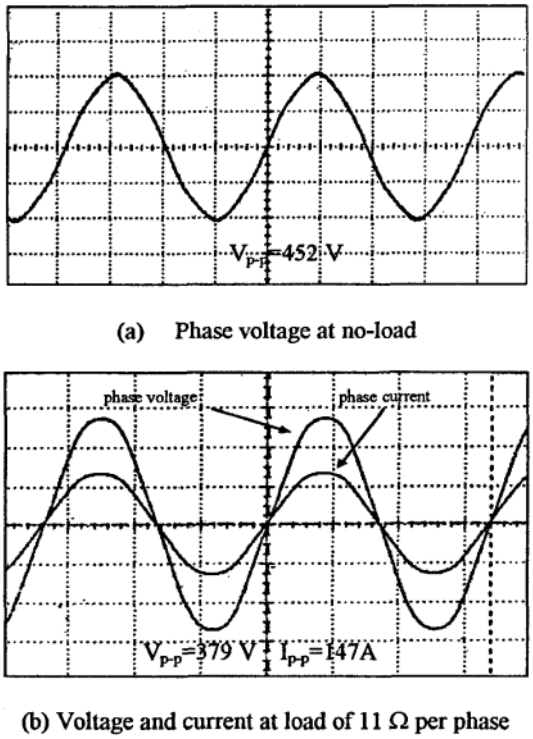

Figure 40 Output waveform [28]

The Fig. 40 shows the difference between waveforms at the no-load test and at the resistive load test of 11R per phase.

Both diagrams of the Fig.40 (a) and (b) were taken at an operating frequency of 68 Hz (170 rpm). The Fig. 40 (a) shows a more standard sinusoidal shape. Since this is related to the properties of the magnet material and the symmetry of the machine, it is will be further studied with finite element analysis.

A comparison of performances is made between the computational and measured results. The design parameters, methods and a proper phasor diagram have been used to predict the output characteristics. The analytical and measured values of output phase voltage versus load current at 6 different speeds are shown in Fig. 41. Compared with the Xd and Xq, at low operating frequency, stator armature resistance ra, has a significant influence on the performance of the permanent magnet machine. It can be Seen in Fig. 41 that, by taking account of ra, the predicted values of regulation at relative lower rotational range keeps a satisfied agreement with the measured ones.

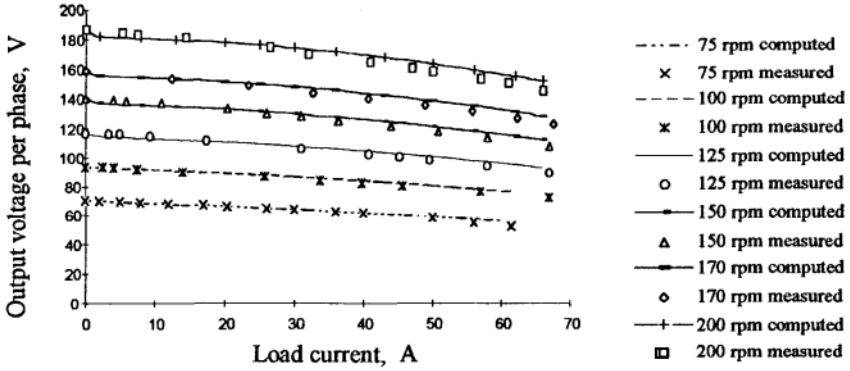

Figure 41 Comparison of regulation [28]

Both curves at the 6 speeds show a positive regulation. The computed results include stator resistance r, and armature reaction with influence of Xq. A good agreement between computations and measurements is obtained within normal load current range. As the load current increased, so did the difference between the predicted and measured voltages. There are two possible reasons:

(a) Variation of stator armature resistance due to temperature rises. In the computation, a constant resistance re at unchanged temperature is only used. But, increased current yielded higher temperature rise and caused the ra to vary in the test.

(b) When frequency increased, load angle and power factor angle varied in a more complicated function, which is related to the features of magnetic material and the symmetry of the machine.

In conclusion above performance described the design of a DDPM Machine, outer-rotor, permanent magnet generator for wind turbine application. A prototype machine was built and tested. It is seen that a 20-kW permanent magnet generator made in such construction can be easily coupled with the wind turbine and operates reliably in an independent wind diesel hybrid generation system. The discussed essential parameters of this machine model can be determined by using computational and experimental methods presented here the reasonable agreement between computed and measured results exhibits the availability of those approaches. [28]

4 Case Study

In this chapter we are going to have a look into the first domestic 2MW direct-drive PMSG system, including optimal machine design, converter topology choosing and its control. The generator injects the power to the grid through two fully controlled back-to-back PWM converters that are parallel connected as master-slave structure. A load current sharing control strategy is presented for the parallel connection. Some experimental results are given to illustrate the performance of the actual system.

Compared to geared drive wind power generation system, direct-drive wind power generation system has the advantages of simplified drive train and increased energy yield, higher reliability and availability and less maintenance by omitting the gearbox. With the development of the permanent magnet material in recent years, permanent magnet (PM) generators with the advantages of higher efficiency and energy yield, no additional power supply for the magnet field excitation and higher reliability due to the absence of mechanical components such as slip rings over the electrically excited machines are used widely in direct-drive wind power generation system. So the PM synchronous generator (PMSG) is a favourite choice in MV class wind power generation system nowadays.

November 2007, the domestic first 2MW direct drive PMSG system was manufactured and operated successfully in Xiangtan Electrical Machine Company (XEMC), which indicated that the design and manufacture of large capacity wind power equipments in our country to a new level.

4.1. Wind Power Generator Optimal Design and Analysis

The direct drive wind power generator operates at low speed of direct connection to the wind turbine, so a larger size and large number of poles of the generator is necessary to deliver a certain power. In this section, electromagnetic design and finite element (FE) analysis of PMSG is discussed

A. Main parameters of PMSG

The main parameters of the designed PMSG are shown in Table 2.

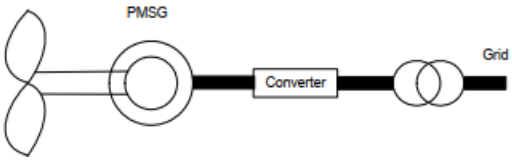

Figure 42 Scheme of a grid-connected PM generator system

Table 2 Main Parameters of PMSG

Rated Power (kW)	2000
Rated Voltage (V)	660
Rated Efficiency (%)	96
Rated Speed (r/min)	22.5
Number of Poles	60
Rated frequency (Hz)	11.25

B. Armature Design

Fig.43 illustrates the size of stator and slot of a PMSG. The outer diameter and inner diameter of stator are 3800mm and 3400mm separately, and the length of stator core is 1400mm. There are 288 slots around the stator core; the height and width are 80mm and 17.2mm. So the stator pole distance τ1can be calculated by

$$\tau_1 = Z_1/(2p) = 288/60 = 4^4/_5 \quad (39)$$

Where Z1 is the number of stator slots; 2p is the number of poles.

The stator-teeth flux density

$$B_{t1} = B_\delta t_1 L_{ef}/(b_{t1} k_{fe} L_1), \quad (40)$$

the stator-yoke flux density

$$B_{j1} = \Phi_{\delta 0}/(2\, k_{fe} L_1 h_{j1}). \quad (41)$$

Where Bδ is the air-gap flux density, t1 is the distance of a stator teeth, Lef is the equivalent core length, L1 is the length of stator core, kfe is stator core stacking factor, bt1 is stator tooth width, φδ0 is the air-gap flux, hj1 is the calculated height of stator yoke.

C. Poles Design

There are 60 PM poles around the rotor, and the PM material is Nd-Fe-B with the performance parameters in Table 3. The magnet thickness hm as a function of air-gap flux density is given by

$$h_m = B_\delta u_r g_{eff} / B_r \quad (42)$$

Where Br is residual flux density of PM, ur is the relative recoil permeability of PM, geff is the effective air-gap, it can be indicated as

$$g_{eff} = k_\delta (g + h_m / u_r) \quad (43)$$

Where kδ is the carter factor of the stator slots, g is the mechanical length of air-gap. Cogging torque which is the inherit feature of PM machine is produced by the magnetic attraction between the rotor mounted PM and the stator teeth. It is the circumferential component of attractive force that attempts to maintain the alignment between the stator teeth and the PM. The inherent cogging torque is considered as a critical issue for PM wind power generator applications, and a lot of approaches are presented to reduce the cogging torque of PMSG, such as skewing. In this design, a method to reduce the cogging torque called "pole cut" is adopted. A PM pole is cut off a pair of angle in every two PM poles, which can change the distribution of the air-gap flux, and then the cogging torque is reduced.

Table 3 MAIN PARAMETERS OF Nd-Fe-B

Residual Flux density (T)	1.15
Coercive force (kA/m)	915
Maximum Energy Density (kJ/m3)	263.1
Relative Recoil Permeability	1.03

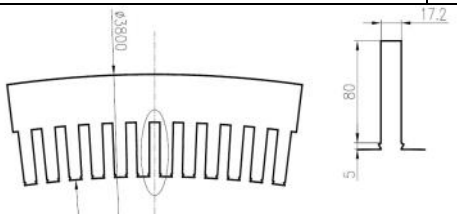

Figure 43 Structure of the stator and slot

D. Data of the electromagnetic design

A 2MW wind power PMSG electromagnetic design data is shown in Table 4 and Table 5.

E. Electromagnetic analysis with Finite Element In order to check the electromagnetic features of above designed 2 MW PMSG, Electromagnetic FE analysis including no-load electromagnetic, rated operation performance and PM demagnetizing feature with the FE program MAXWELL is carried out.

(1) No-load Electromagnetic analysis

Through electromagnetic-static analysis of the designed PMSG 1-pole-pair at no-load operation with the FE program MAXWELL, the static flux distribution of the stator and field curves of the air-gap flux density radial component in the middle of the mechanical air gap along the armature circumferential for one pole pair are obtained. (Fig.44 and Fig.45) The electromagnetic analysis peak value of air-gap flux density shown in Fig.45 is about 0.9T, which accords with the numerically calculated value in Table IV quite well.

Table 4 MAIN DIMENDIONS OF PMSG

Outer diameter of stator (mm)	3800
Inner diameter of stator (mm)	3480
Diameter of air-gap (mm)	5
Length of core (mm)	1300
Number of poles	60
Number of slots	288
Stator slot width (mm)	17.2
Stator slot height (mm)	80
Magnet height (mm)	22
Magnet width (mm)	125

Table 5 MAIN DESIGN DATA OF PMSG

No-load air-gap flux density (T)	0.78
No-load stator teeth flux density (T)	1.68
Rated out power (Kw)	2120
Rated voltage (V)	660
Rated current (A)	1936
Rated power factor	0.98
Rated efficiency (%)	95.1
Rated torque (kN.m)	935

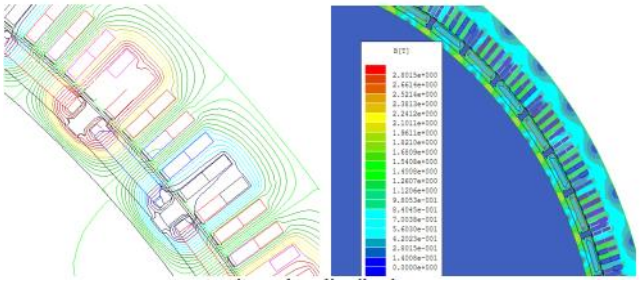

Figure 44 Flux distribution

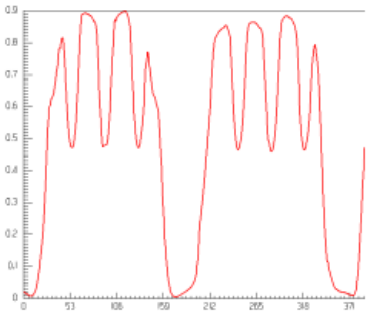

Figure 45 Radial air-gap flux density distribution

(2) Rated operation performance analysis

The rated operation performance on the condition of stator winding connection to separate load and grid is analyzed with the FE models (Fig.46) by FE program MAXWELL. When the PMSG stator winding connects with a separate resistance, the analyzed terminal voltage and winding current waveforms are shown in Fig.47 and

Fig.48.Because of the voltage regulation, the terminal voltage of PMSG is much lower than the rated value, and the winding current is larger than that on the condition of connecting to the grid. By analysis, the maximum output power when connecting with a separate resistance attains to 2.03MW, and the efficiency is 94.5%, the winding current is 2751.2A.

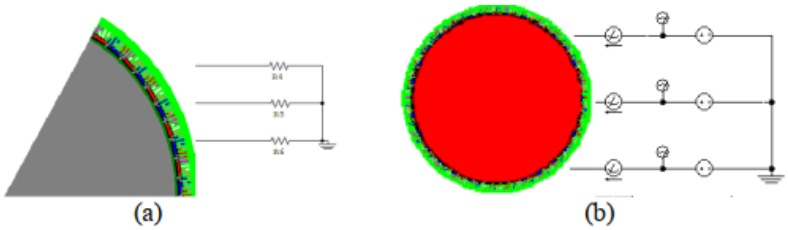

Figure 46 Analysis model of PMSG

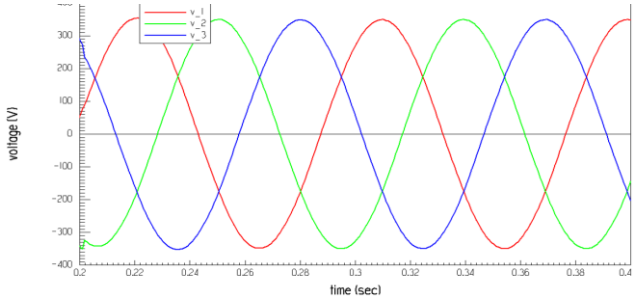

Figure 47 Terminal voltage on the condition of connecting to a resistance

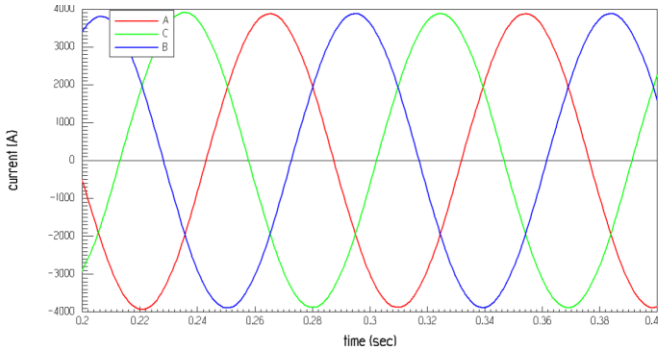

Figure 48 Winding current on the condition of connecting to a resistance

When the PMSG stator winding connects to the grid, which keeps a constant value, the analyzed terminal voltage and winding current waveforms are shown in Fig.49 and Fig.50. On this condition, the terminal voltage keeps the value with the grid, and the maximum power delivering to the grid can attain to 2.12MW

(3) Demagnetizing feature of PM analysis

In order to check the magnetic performance of the selected PM material, the demagnetized feature of Nd-Fe-B is analyzed on the condition of no-load, rated-load and short operation. The flux density of PM material is shown in Fig.51, and the flux density values of PM material on above conditions are 0.9T, 0.74T and 0.55T.

From above analysis, we can conclude that: (1) when the designed PMSG operating connected to the grid, the maximum output electrical power can attain to 2.12MW, and has the perfect performance; (2) when the designed PMSG operating connected with a separate load, the maximum output electrical power can attain to 2.03MW, and the terminal voltage declines nearly 30% compare with the grid voltage; (3) when the designed PMSG operating on short condition, the flux density of selected PM material still keeps 0.55T, which indicates perfect demagnetizing feature.

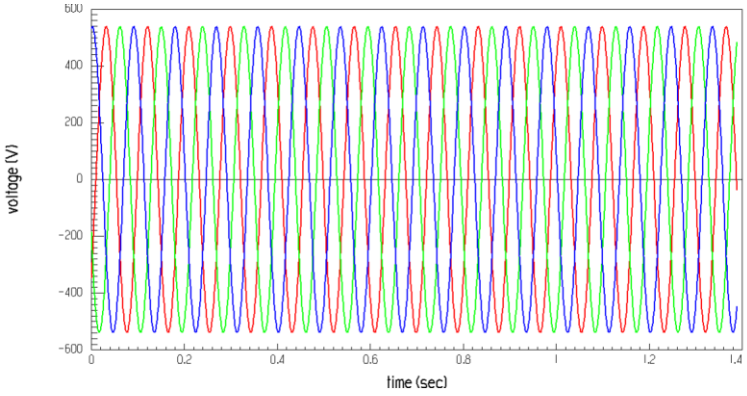

Figure 49 Terminal voltage on the condition of connecting to grid

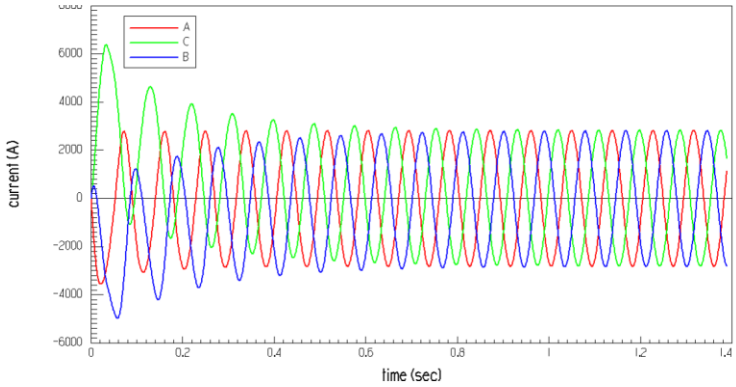

Figure 50 Winding current on the condition of connecting to grid

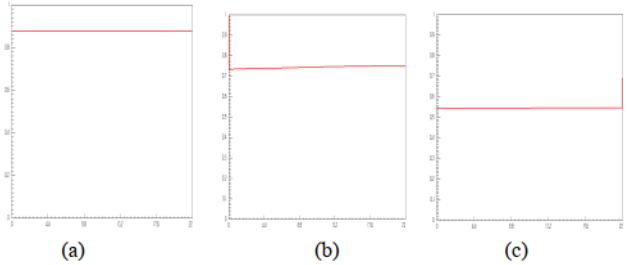

Figure 51 Flux density of PM material

(a) no-load (b) rated load (c) short operation

4.2. Configuration And Control of The Converters

In order to attain large capacity converter for the full power transformation, two 1MW back-to-back PWM converters with parallel connection are used to feed the power to the grid. In this section, the configuration, structure and control strategy of the converter are discussed.

A. Structure of the parallel converter

The scheme of a 2MW full power converter which can be used as the interface between the stator of PMSG and grid is shown as Fig.52. In order to deliver 2MW power energy to grid, two separate1MW back-to-back converters including generator-side converter and grid-side converter with the same scheme are connected in parallel. There are five controllers working together to realize the control of generator-side and grid-side currents, grid-side power factor and DC bus voltage. Master-slave control strategy is adopted: A master controller is used to communicate with centre system, to give current reference to converter controllers of each branch and as interface with persons. The other four slave controllers' duty is to control generator-side and grid-side converters of each branch. In order to omitting loop current between the two branches, the master controller gives the same q-axis current reference to generator-side converter controllers of each branch.

B. Converter control strategy

The PMSG is controlled by generator-side converter controllers in a rotor rotating dq axis frame, with the d-axis oriented along the rotor-flux vector position. In this way, the d-axis current is held to zero to obtain maximum electromagnetic torque with minimum current. In order to omitting loop current between the two branches, the two generator-side converters get the same current reference from the master controller. The generator-side converters control strategy scheme can be seen as Fig.53. The required d-axis current component keeps zero; the required q-axis current component is derived from the speed loop of master controller. The control needs the measurement of the stator current and the rotor position. Space-vector modulation is used to generate the switching signals for the power converter semiconductors.

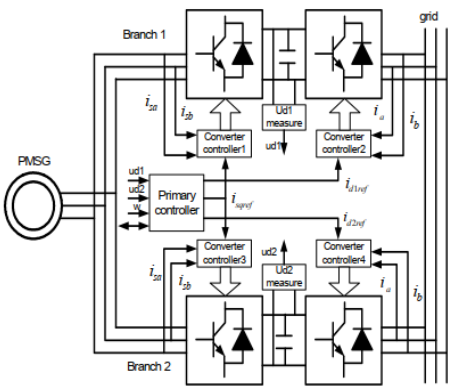

Figure 52 Structure of the parallel connection converter

The objective of grid-side converter is to enable independent control of the active and reactive power flowing to the grid. The required d-axis current component is derived from the DC-link voltage loop of the master controller; the reactive power reference decides the required q-axis current component. The control in the synchronous dq axis frame needs the measurement of the grid current. The Space-vector modulation is quite similar to that of the generator. The grid-side converters control strategy scheme can be seen as Fig.54.

To release the calculation of the four converter controllers, the Master controller is to keep the DC-link voltage constant, calculate the q-axis current component reference of PMSG, and do some other work with the center system. The master controller communicates with the other slave controllers by the CAN-bus. The Master control strategy scheme can be seen as Fig.55.

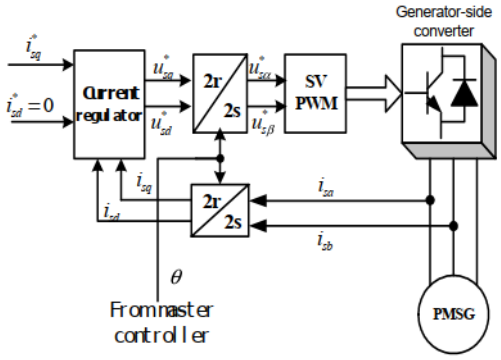

Figure 53 Control scheme of the generator-side converter

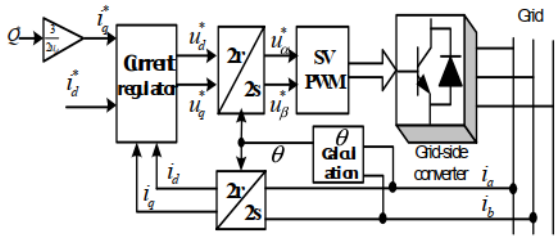

Figure 54 Control scheme of the grid-side converter

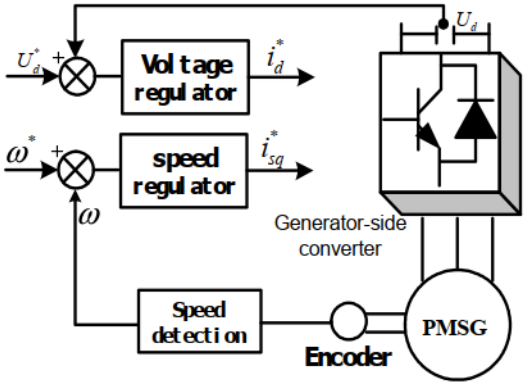

Figure 55 Control scheme of the master converter

4.3. Simulation And Experimental Analysis

For demonstrating the feasibility of above-mentioned control strategy simulation work with Matlab/simulink has been performed. The simulation data is given in Table 6. [30]

Table 6 SIMULATION DATA OF PMSG

Rated power (Kw)	2000
Number of poles	60
Rated Voltage (V)	660
Rated Speed (r/min)	22.5
Rated power factor	0.95
Stator resistance (Ω)	0.00665
D-axis reactor (Ω)	0.094
Q-axis reactor (Ω)	0.163
DC link voltage (V)	650

To testify the validity to omitting the loop current between the two converter branches of the master-slave control model, another simulation of parallel control model, which means the two converter branches are controlled separately, as a contrast is also carried out.Fig.56 and Fig.57 show the curves of (a) Generator-side converter currents, (b) Sum of two generator-side branches currents, (c) Difference of two generator-side branches currents and (d) Three phase currents of PMSG of master-slave and parallel control model. From the currents curves, we can see that the stator currents and the branch currents are quite same with each other of the two control models, but the currents difference of the two parallel converter branches (Fig.(c)) are quite different. The currents difference on master-salve control model is much smaller than that on parallel control model. So it is obvious that the master-slaver control model is more effective to restrain the current loop between the two parallel convert branches. [30]

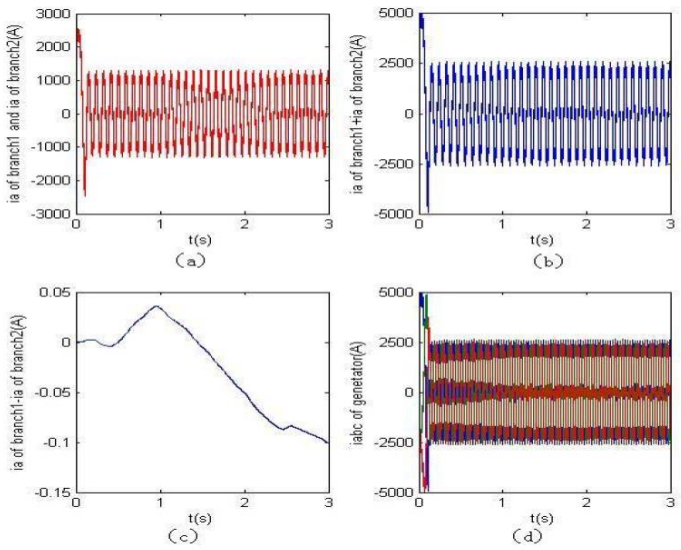

Figure 56 Currents curves on master-slave control model (a) Generator-side converter currents of two branches; (b) Sum of two generator-side branches currents; (c) Difference of two generator-side branches currents; (d) Three phase currents of PMSG [30]

Fig.57 shows the two phases currents of PSMG, which are close to sinusoidal waves. Fig.58 shows the currents and voltage of the grid-side converter, which suggests that the grid-side current and voltage waveforms are very close to sinusoidal waves and power factor is nearly equated to 1. The grid-side currents of each converter branch are shown as Fig.59. The two branches currents are nearly the same both in value and phase, which indicate the current loop between the two converter branches is controlled well. The above three waveforms demonstrate that the designed and produced 2MW PMSG system can indeed achieve the anticipative targets, and has good electrical performance. [30]

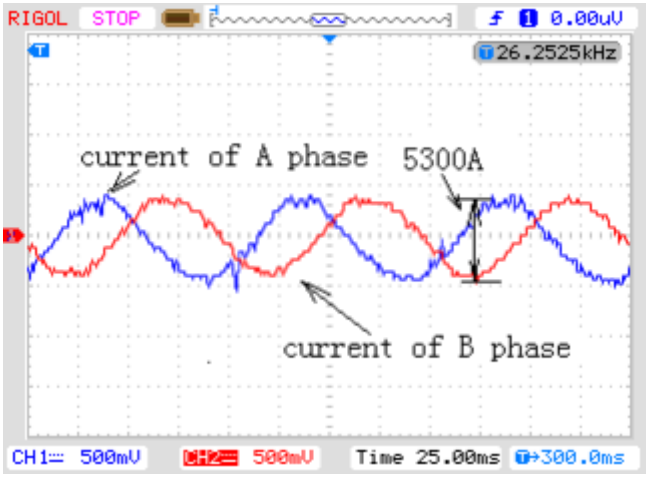

Figure 57 Phase currents of PMSG

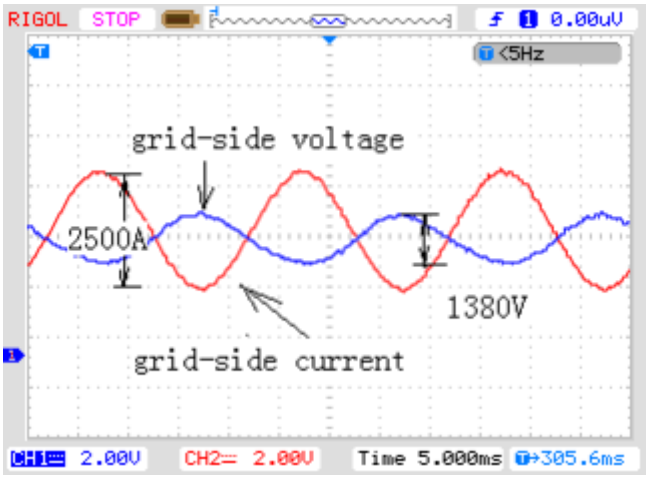

Figure 58 Voltage and current of grid-side converter

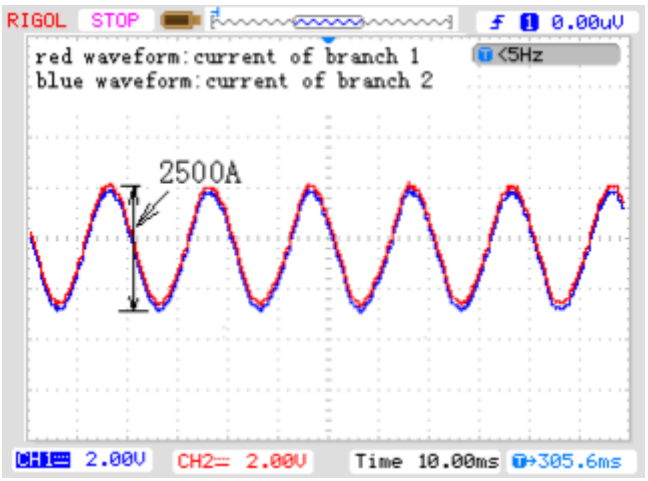

Figure 59 Grid-side currents of each converter branch

The engineering design and the control strategy for an actual 2MW direct-driven permanent magnet synchronous generator fed by parallel-connected full power back-to-back PWM converters have been discussed. The optimal generator design and electromagnetic EF analysis are carried out for wind generation application. Two back-to-back converters with parallel connection are used to enlarge the capacity. Vector-control techniques have been applied to both machine-side and grid-side converters. The structure, control scheme and simulation analysis of a 2MW full power parallel connection converter are discussed. [30]

5 Conclusion

In conclusion, by mechanical point of view, the solution for reducing the mechanical structure, DDPM for large wind turbines is to do without a shaft and torque arms. In thermal aspects, some main parameters for design like polar arc coefficient and air gap length on various parts of AFPM and RFPM were compared and studied, and we can conclude that, variations in heat source and thermal resistance are the fundamental causes of temperature changes. The majority of the characteristics used as the study object in this work have an impact on both the heat source and thermal resistance. For Electromagnetic design, we discussed both static and dynamic operation of PM machines and some of the machine performance aspects are mentioned.

Finally, we have discussed the case study of 2MW DDPMSG fed by PMW converters and it shows that the performance of DDPM is good and reliable.

The design of the PM machines is a bit complex but the higher power efficiencies can be achieved by this technology. PM Machines for wind turbine gives reliability and profit in long run.

5.1. Future Development

In this thesis, the permanent magnet generator of 2MW could be studied further along with its electrical characteristics like short circuit studies to understand better and in detail. In future the Permanent magnet machines could have a promising future due to its performance and long run efficiency and profitability. In these days the IM are mostly used because of their short-term compatibility but, when we see in a long run, PMSG could be solution for the wind industry.

Bibliography

[1] Neill, S.P.; Hashemi, M.R. Offshore Wind. In Fundamentals of Ocean Renewable Energy; E-Business Solutions; Academic Press: Cambridge, MA, USA, 2018; pp. 83–106.

[2] Tong, W. Fundamentals of Wind Energy. In Wind Power Generation and Wind Turbine Design; WIT Press: Southampton, UK, 2010; p. 23.

[3] Dykes, K.; Platt, A.; Guo, Y.; Ning, A.; King, R.; Parsons, T.; Petch, D.; Veers, P. Effect of Tip-Speed Constraintson the Optimized Design of a Wind Turbine; Technical Report; National Renewable EnergyLaboratory (NREL): Golden, CO, USA, 2014.

[4] Johnson, K.; Fingersh, L.; Balas, M.; Pao, L. Methods for Increasing Region 2 Power Capture on a Variable Speed HAWT. In Proceedings of the 42nd AIAA Aerospace Sciences Meeting and Exhibit, Reno, Nevada, 5–8 January 2004.

[5] Wang, N. Advanced Wind Turbine Control; Hu, W., Ed.; Springer: Cham, Switzerland, 2018; pp. 281–297.

[6] https://www.vectorenewables.com/en/media-en/blog/types-of-wind-turbines-which-one-generates-the-most-energy

[7] https://www.researchgate.net/figure/Overview-of-main-components-for-a-wind-turbine_fig2_318112329

[8] https://energyeducation.ca/encyclopedia/Types_of_wind_turbines

[9] http://xn--drmstrre-64ad.dk/wp content/wind/miller/windpower%20web/en/tour/design/updown.html

[10] https://hal.science/hal-01213120/document

[11] http://www.egr.unlv.edu/~eebag/SynchronousGenerator

[12] https://core.ac.uk/download/pdf/144730459.pdf

[13] https://www.issr-journals.org/xplore/ijias/0004/003/IJIAS-13-235-04.pdf

[14] https://ieeexplore.ieee.org/stamp/stamp.jsp?tp=&arnumber=9020274

[15] C.E.A. Silva, D. S. Oliveira Jr., L.H.S.C. Barreto, R.P.T. Bascopé, "A Novel Three-phase Rectifier with High Power Factor for Wind Energy Conversion Systems", Power Electronics Conf., 2009, COBEP '09, pp. 985-992

[16] https://ietresearch.onlinelibrary.wiley.com/doi/epdf/10.1049/elp2.12218

[17] https://www.ijrti.org/papers/IJRTI1707021.pdf

[18] https://repository.lib.ncsu.edu/handle/1840.20/35393

[19] https://ieeexplore.ieee.org/stamp/stamp.jsp?tp=&arnumber=1058105

[20] P.J. Tavner and E. Spooner, "Light structures for large low-speed machines for direct-drive applications", in Proc. of the International Conference on Electrical Machines(ICEM), pp. 421.1-6, September 2006

[21] Deok-je BANG, "Design of Transverse Flux Permanent Magnet Machines for Large Direct-Drive Wind Turbines", Ph.D. thesis, Pukyong National University.2010.

[22] S. Engström and S. Lindgren, "Design of NewGen direct-drive generator for demonstration in a 3.5 MW wind turbine", EWEC (European Wind Energy Conference & Exhibition, Milan, Italy, May 7-10 2007.

[23] ENERCON GmbH, http://www.enercon.de/en/_home.htm, last accessed November 2006

[24] A.S. McDonald, M.A. Mueller and H. Polinder, "Comparison of generator topologies for direct-drive wind turbines including structural mass", in Proc. of the International Conference on Electrical Machines(ICEM), pp. 360.1-7, September 2006

[25] STX Windpower B.V., http://www.stxwind.com/nl/products/7-products, last accessed June 2010

[26] https://ieeexplore.ieee.org/stamp/stamp.jsp?tp=&arnumber=8921535

[27] K.S. Ball, B. Farouk, V.C. Dixit, "An experimental study of heat transfer in a vertical annulus with a rotating inner cylinder," International Journal of Heat and Mass Transfer, vol. 32, no. 8, pp. 1517-1527, 1989

[28] https://ieeexplore.ieee.org/document/702743

[29] Hongsinge, V.B.:'The fields and parametes of interior type a.c. permanent magnet machines', IEEE Trans.,

1982, PAS-101, (4), pp.867-876

[30] https://ieeexplore.ieee.org/document/4771139